# Redox Isomeric Ferrocenyl Styrylruthenium Radical Cations with Diphenyl-Substituted β-Ketoenolato Ligands

Christopher Hassenrück,[a] Mykhailo Azarkh,[a] Malte Drescher[a], Michael Linseis,[a] Serhiy Demeshko,[b] Franc Meyer,[b] and Rainer F. Winter*[a]

[a] University of Konstanz, Department of Chemistry, Universitätsstraße 10, 78457 Konstanz, Germany

[b] Georg-August-Universität Göttingen, Institut für Anorganische Chemie, Tammannstraße 4, 37077 Göttingen, Germany

*Supporting Information*

**NMR spectra**

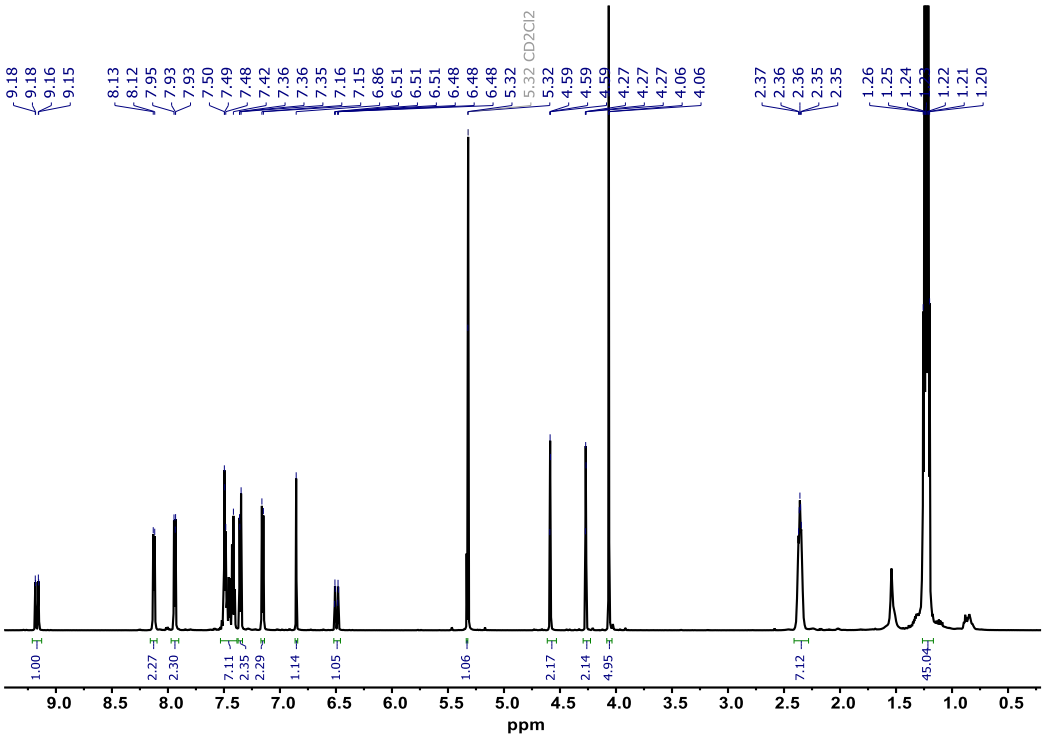


Figure S1. $^{1}$H NMR spectrum of **2-H** in $CD_2Cl_2$ at room temperature.

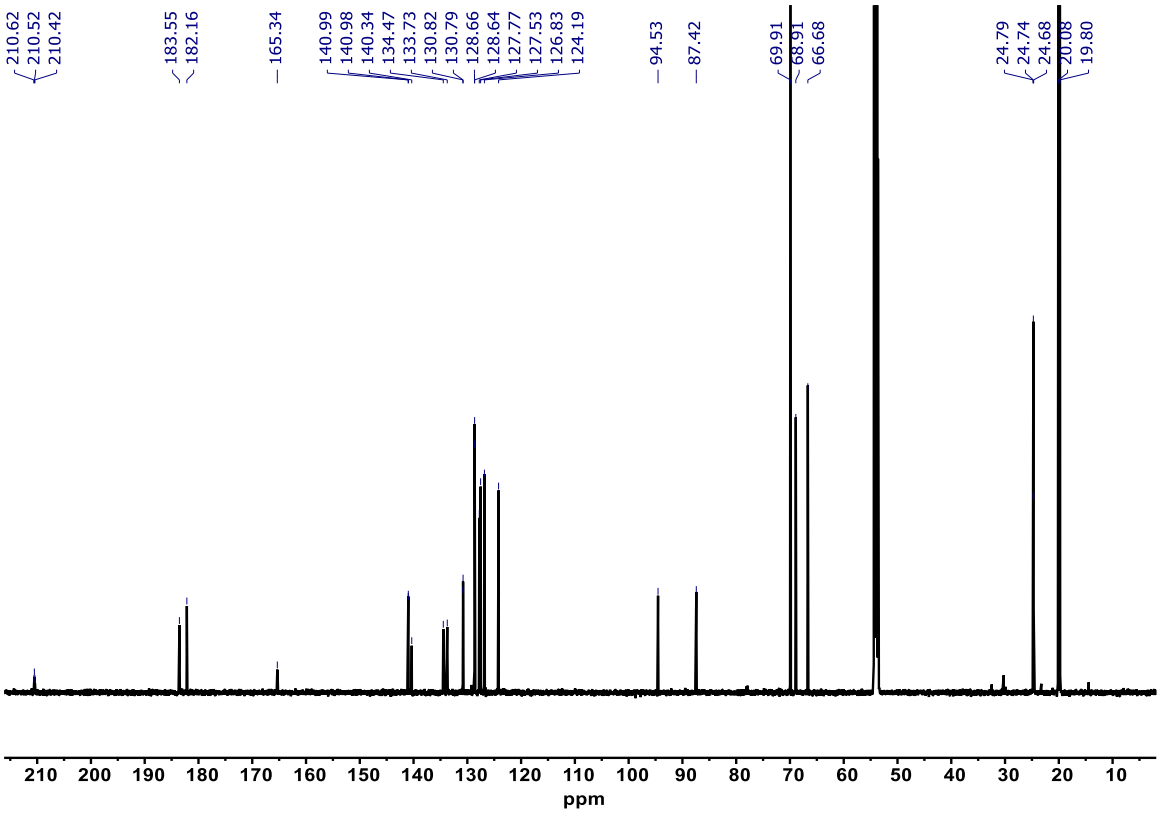


Figure S2. $^{13}C$ NMR spectrum of **2-H** in $CD_2Cl_2$ at room temperature.

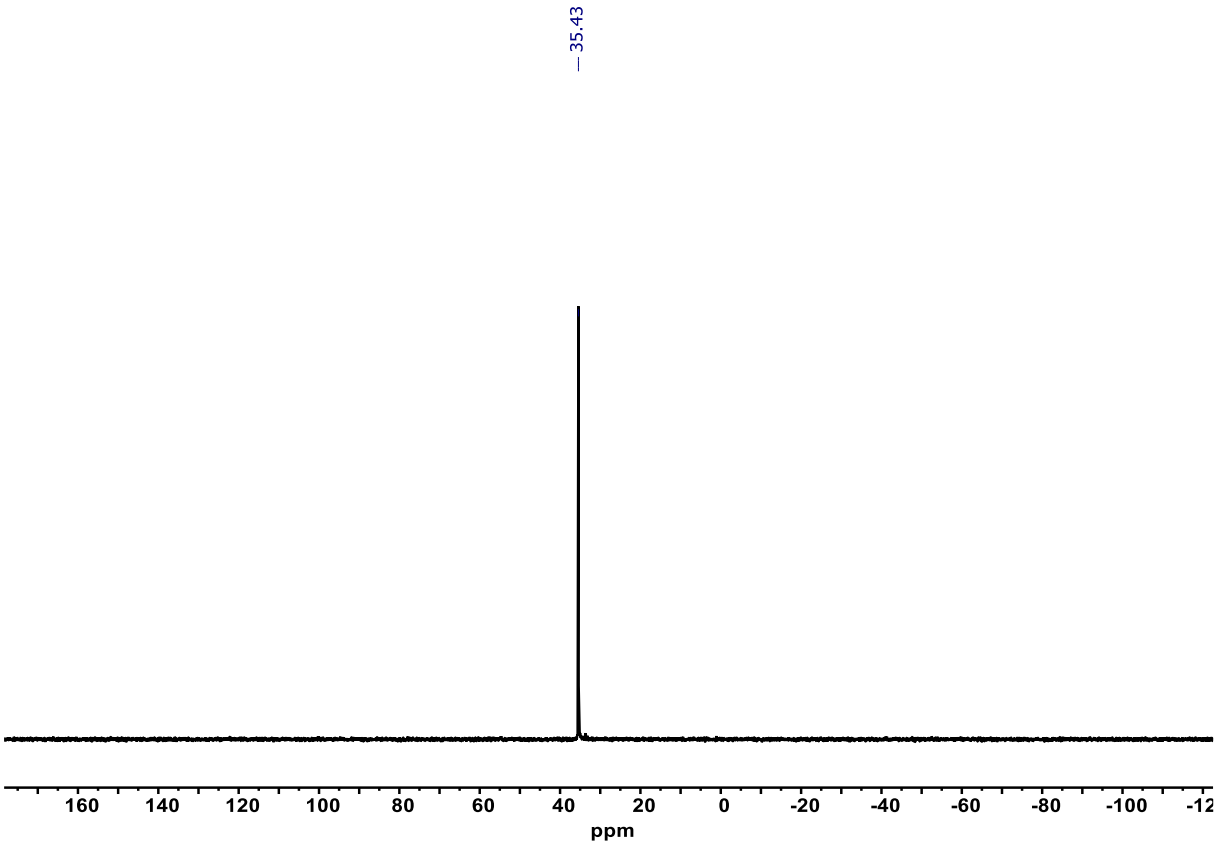


Figure S3. $^{31}P$ NMR spectrum of **2-H** in $CD_2Cl_2$ at room temperature.

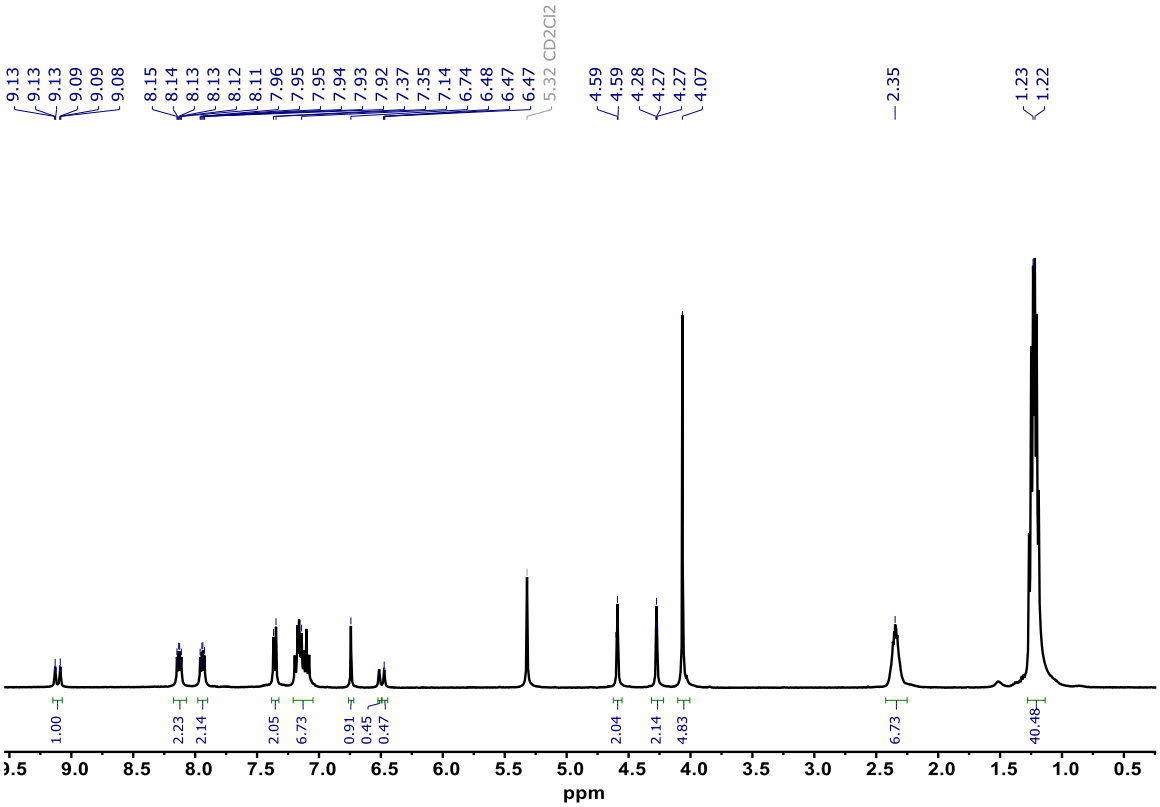


Figure S4. $^{1}H$ NMR spectrum of **2-F** in $CD_2Cl_2$ at room temperature.

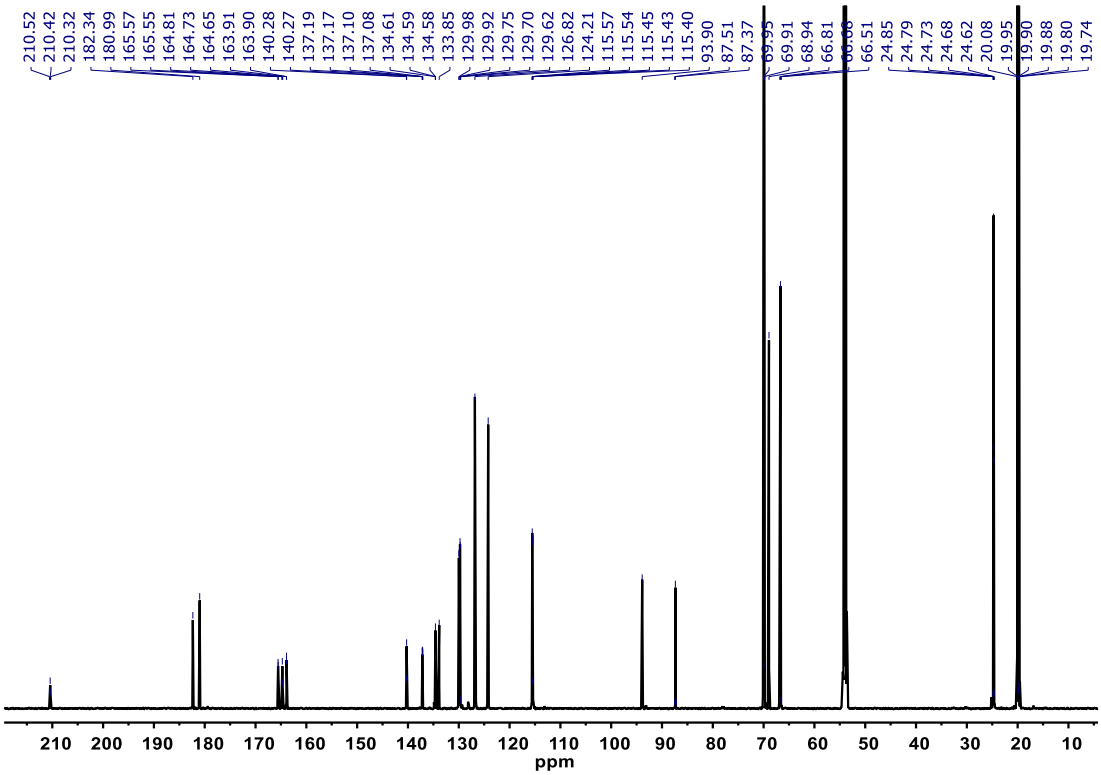


Figure S5. $^{13}C$ NMR spectrum of **2-F** in $CD_2Cl_2$ at room temperature.

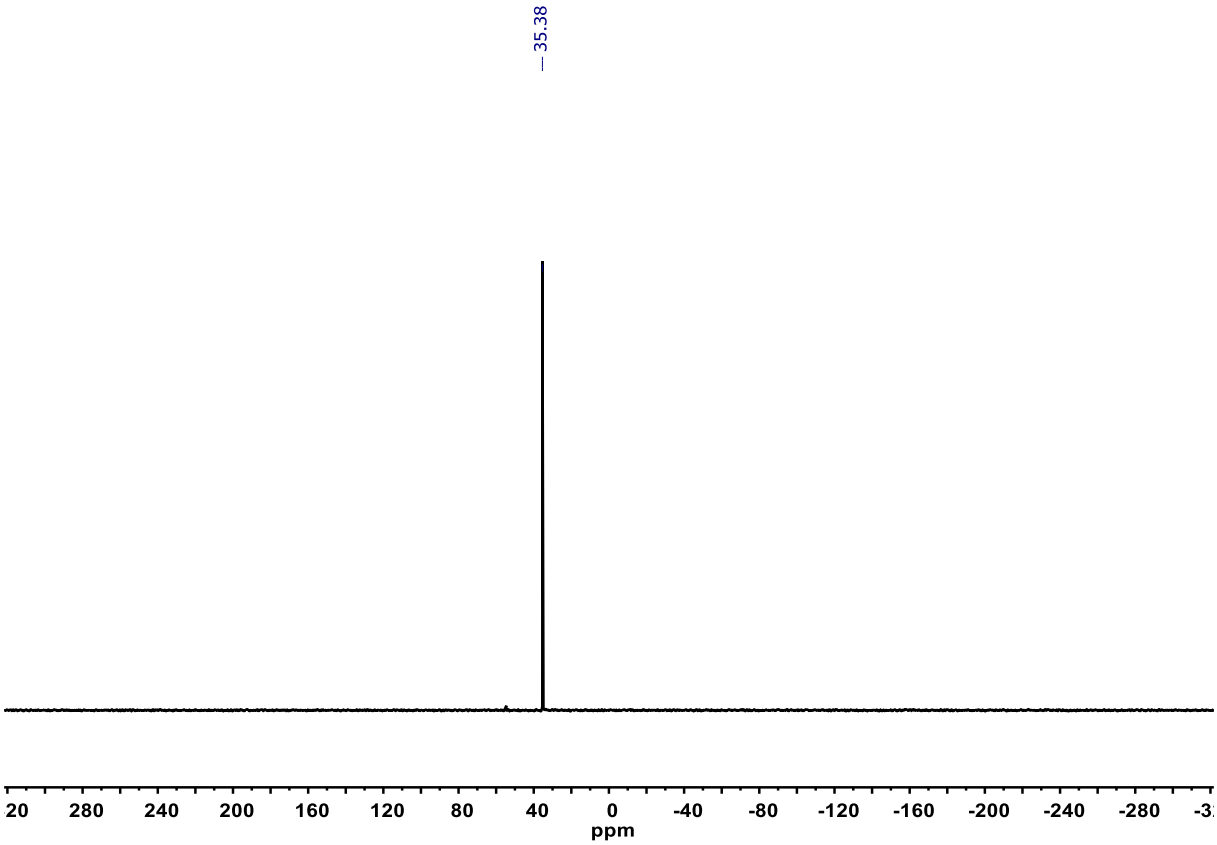


Figure S6. $^{31}P$ NMR spectrum of **2-F** in $CD_2Cl_2$ at room temperature.

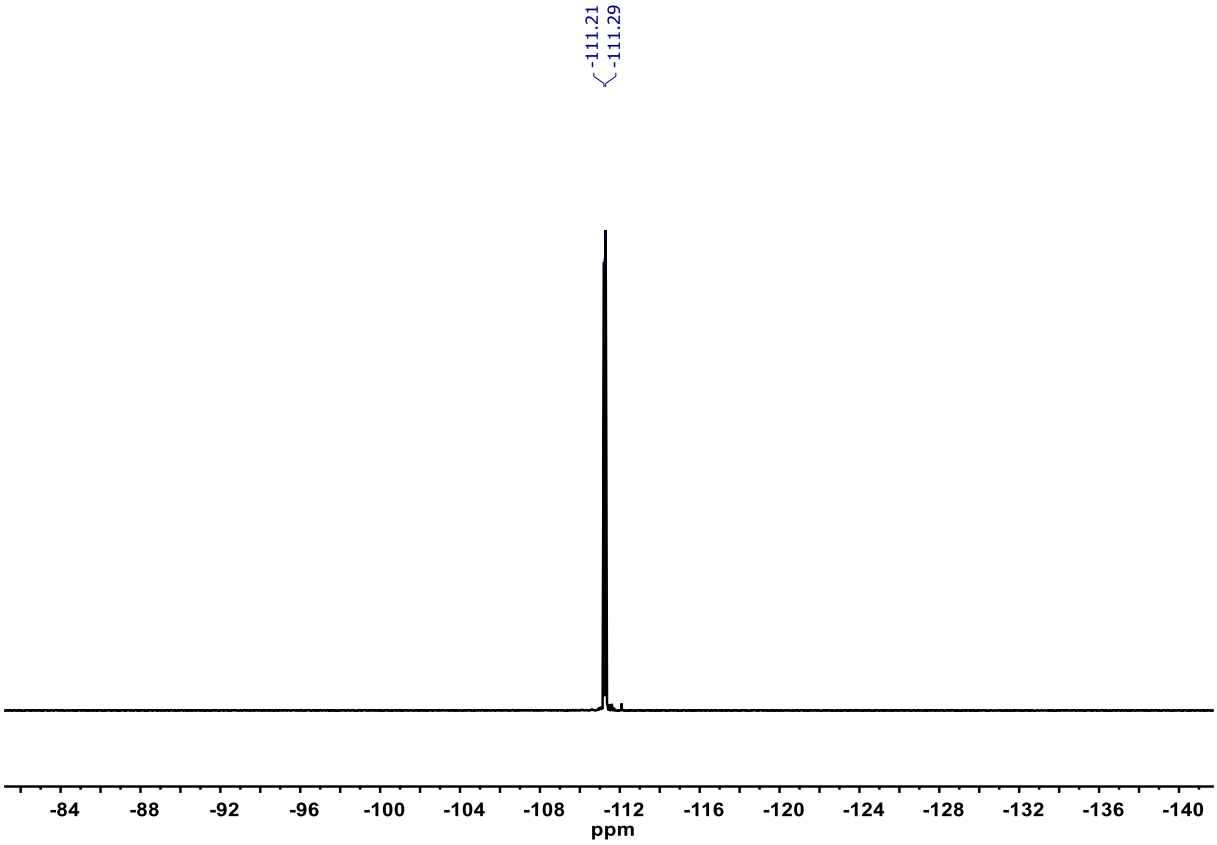


Figure S7. $^{19}F$ NMR spectrum of **2-F** in $CD_2Cl_2$ at room temperature.

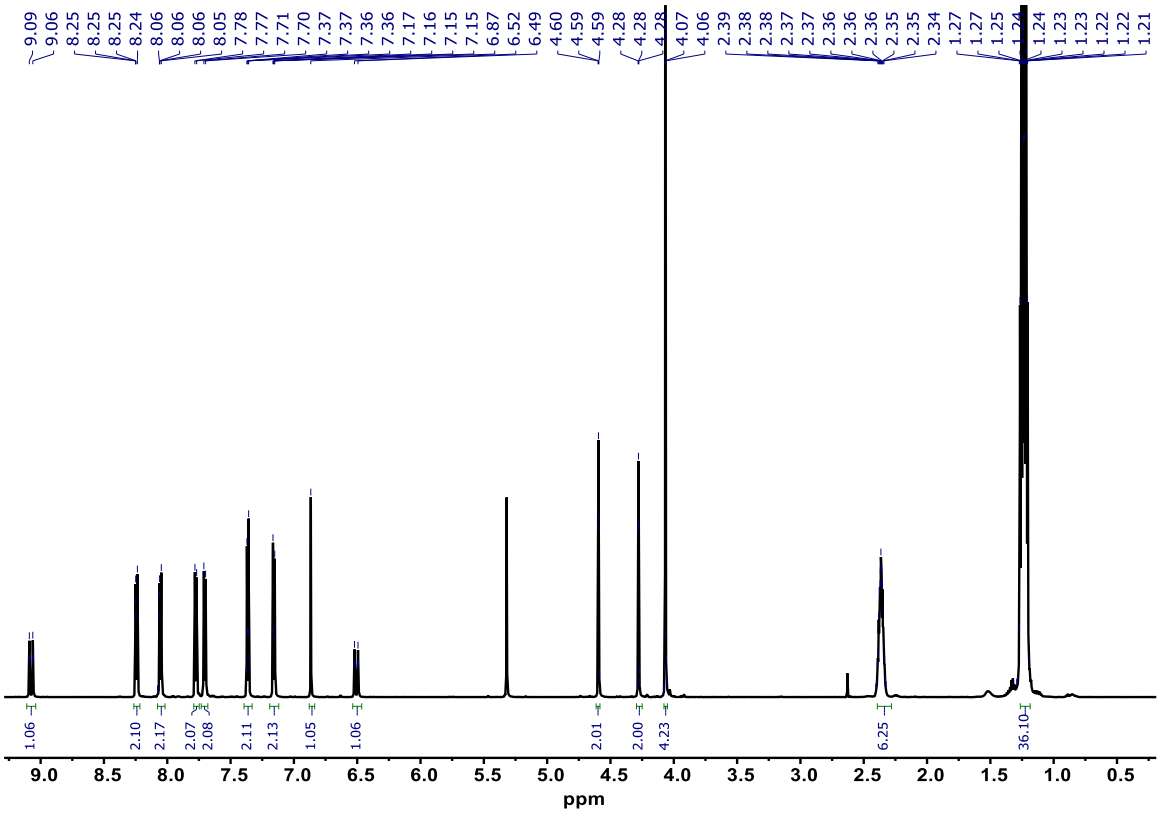


Figure S8. $^{1}H$ NMR spectrum of **2-$CF_3$** in $CD_2Cl_2$ at room temperature.

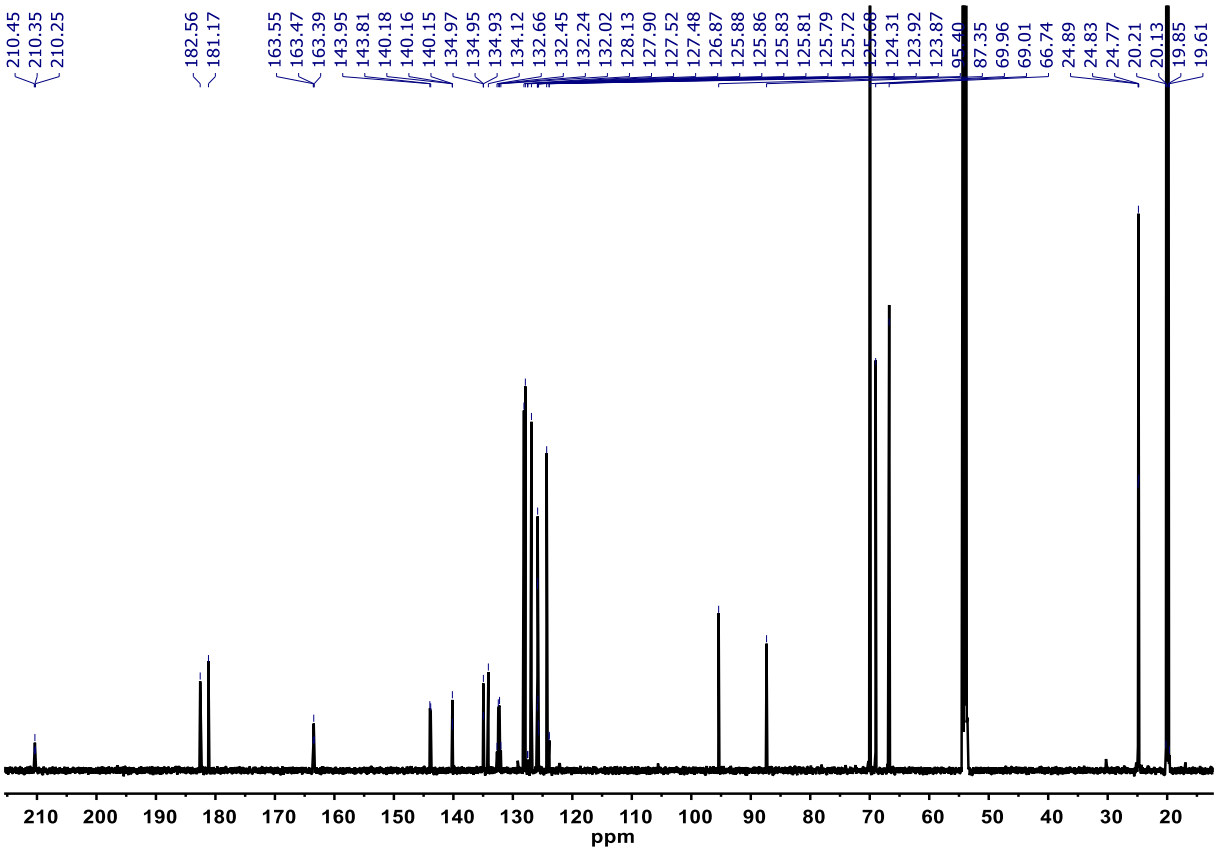


Figure S9. $^{13}C$ NMR spectrum of **2-$CF_3$** in $CD_2Cl_2$ at room temperature.

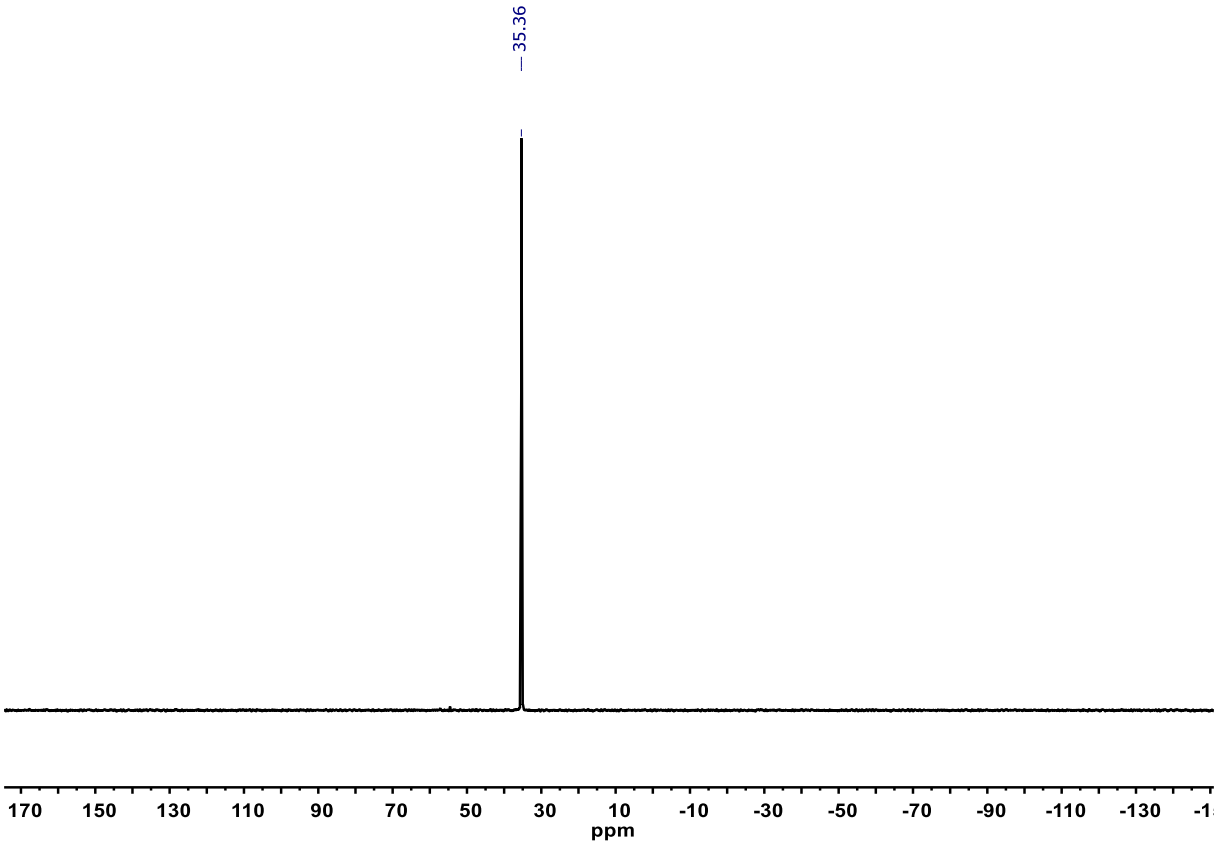


Figure S10. $^{31}P$ NMR spectrum of **2-$CF_3$** in $CD_2Cl_2$ at room temperature.

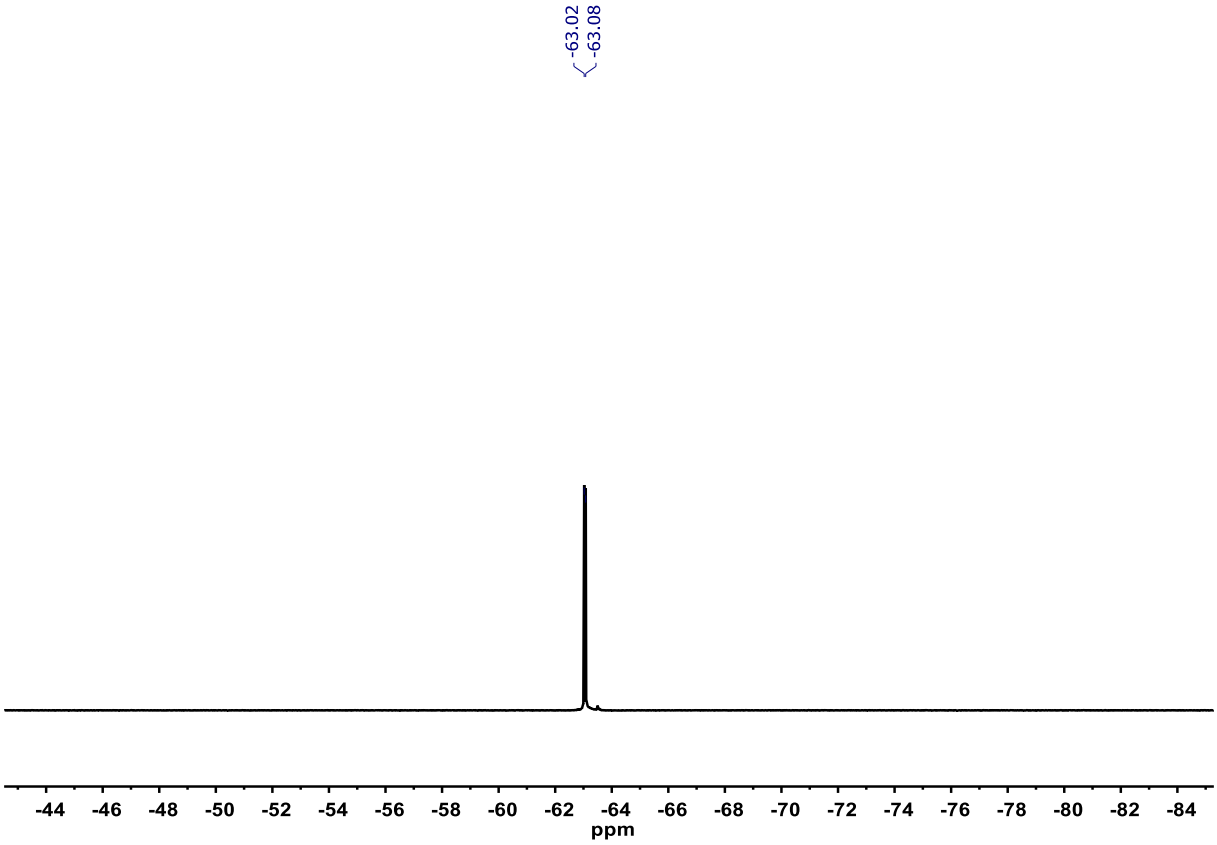


Figure S11. $^{19}F$ NMR spectrum of 2-$CF_3$ in $CD_2Cl_2$ at room temperature.

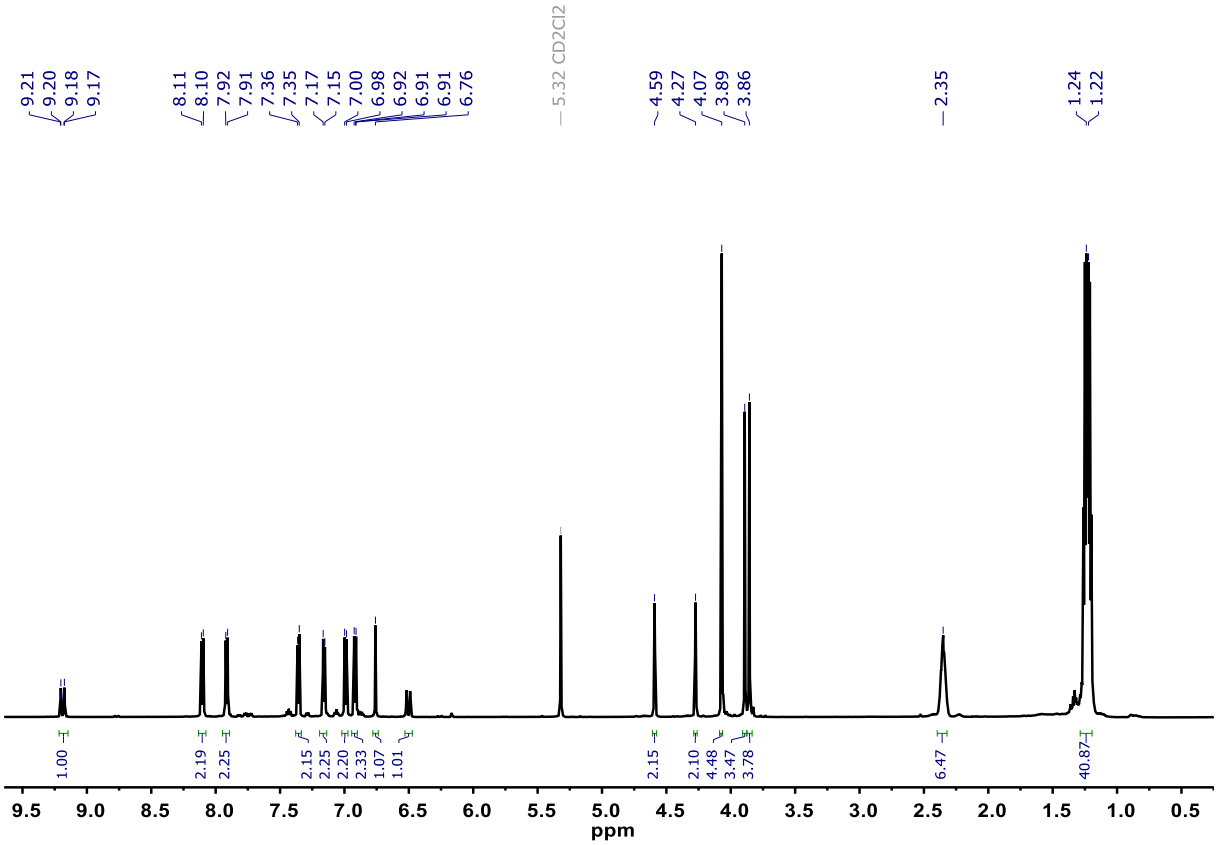


Figure S12. $^{1}H$ NMR spectrum of **2-OMe** in $CD_2Cl_2$ at room temperature.

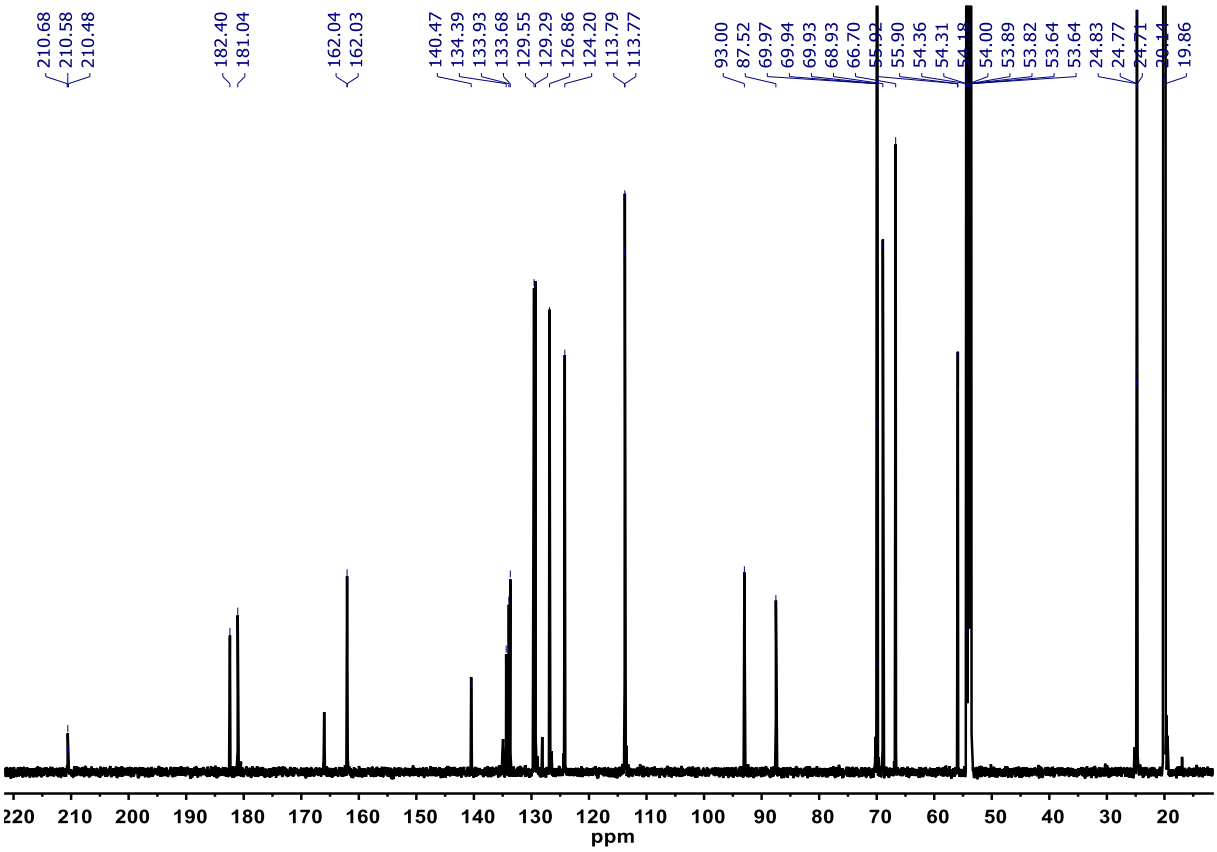


Figure S13. $^{13}C$ NMR spectrum of **2-OMe** in $CD_2Cl_2$ at room temperature.

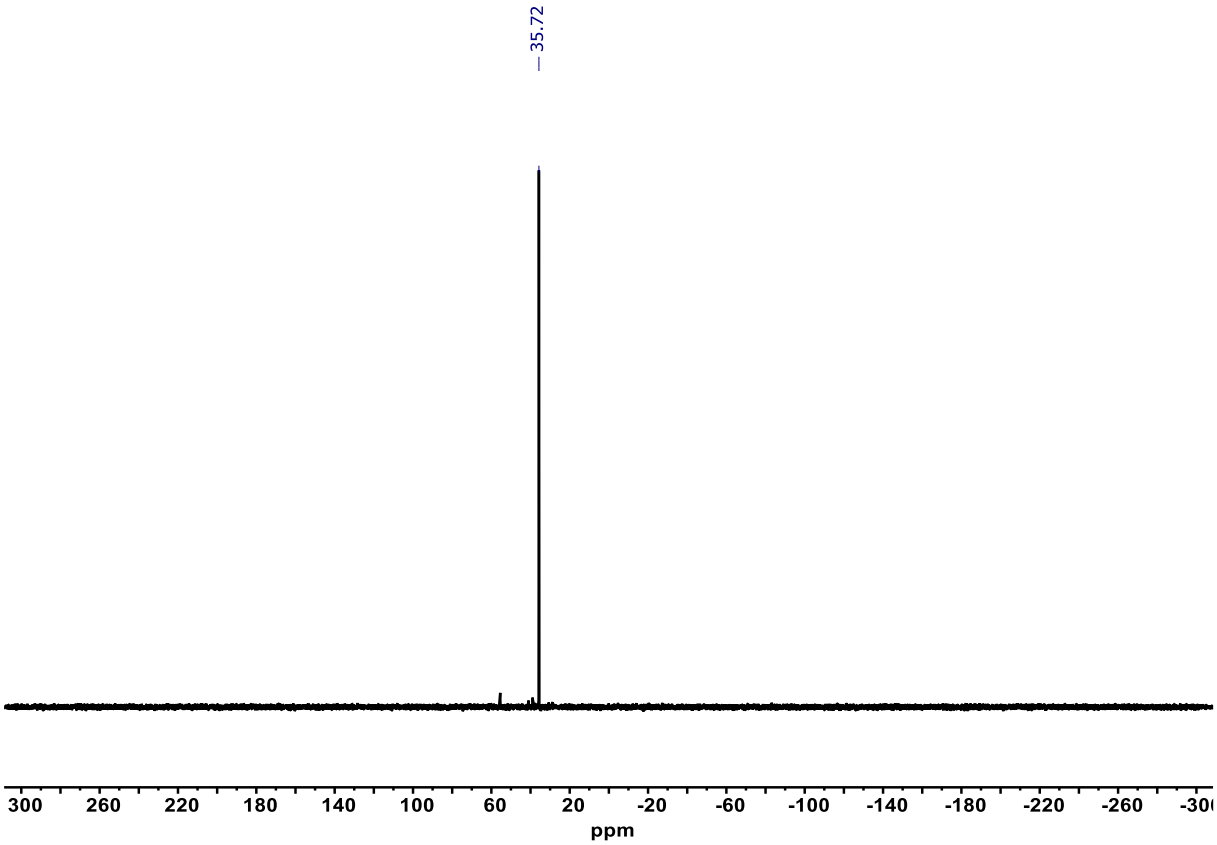


Figure S14. $^{31}P$ NMR spectrum of **2-OMe** in $CD_2Cl_2$ at room temperature.

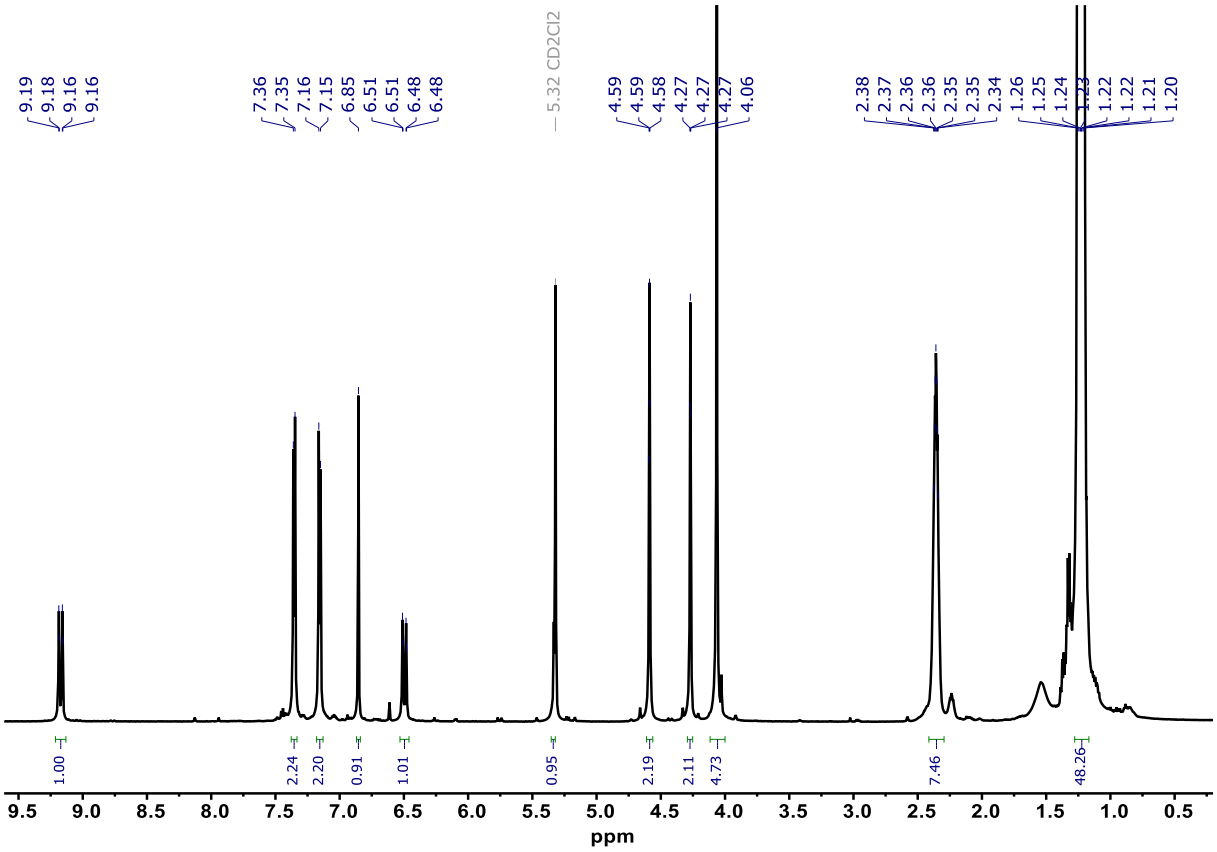


Figure S15. $^{1}H$ NMR spectrum of **2-D** in $CD_2Cl_2$ at room temperature.

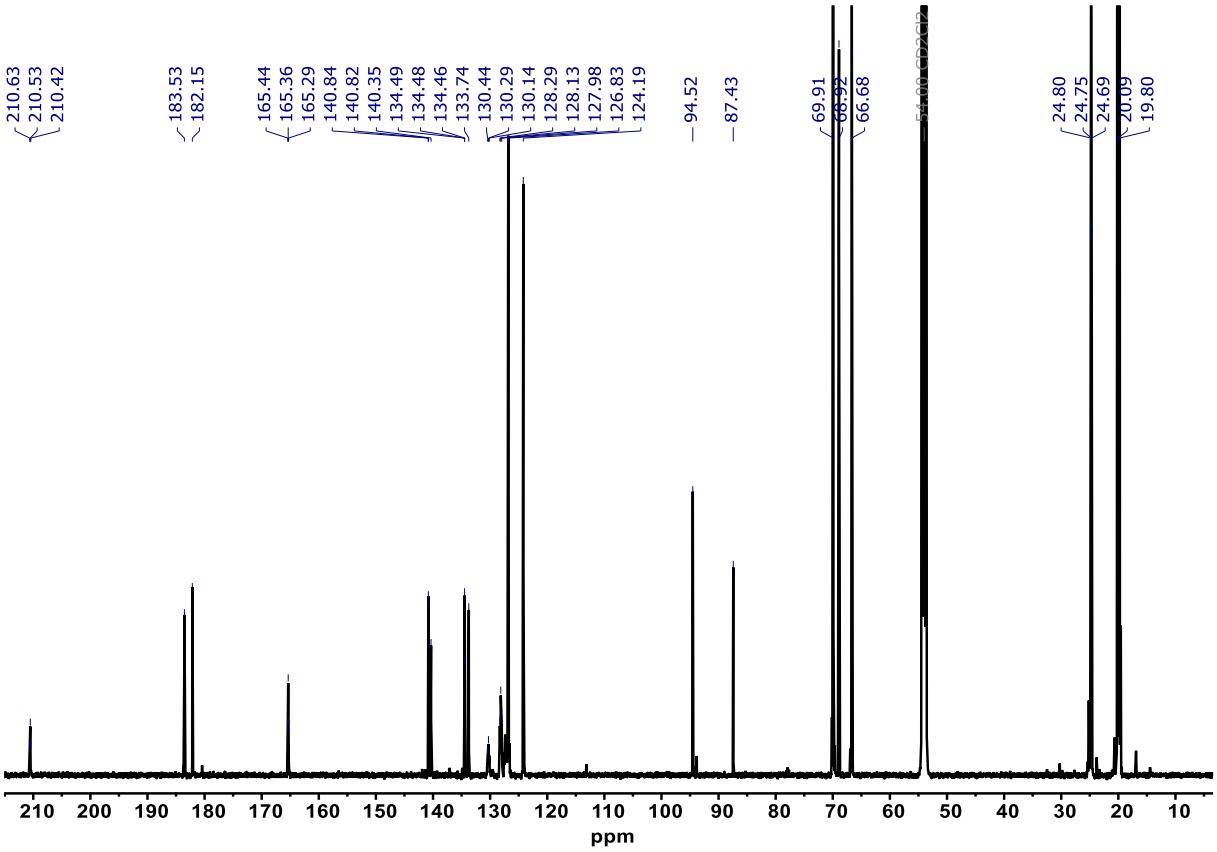


Figure S16. $^{13}C$ NMR spectrum of **2-D** in $CD_2Cl_2$ at room temperature.

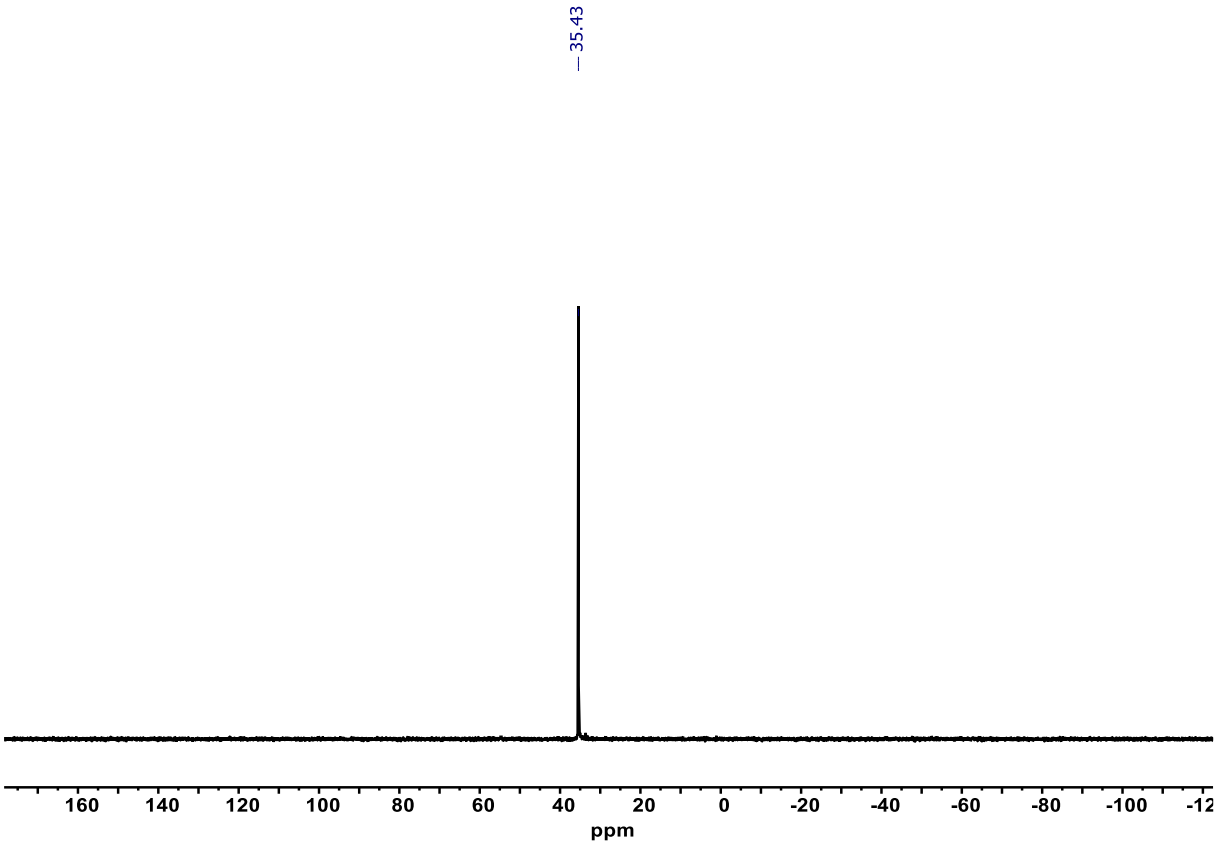


Figure S17. $^{31}P$ NMR spectrum of **2-D** in $CD_2Cl_2$ at room temperature.

## X-ray diffraction study

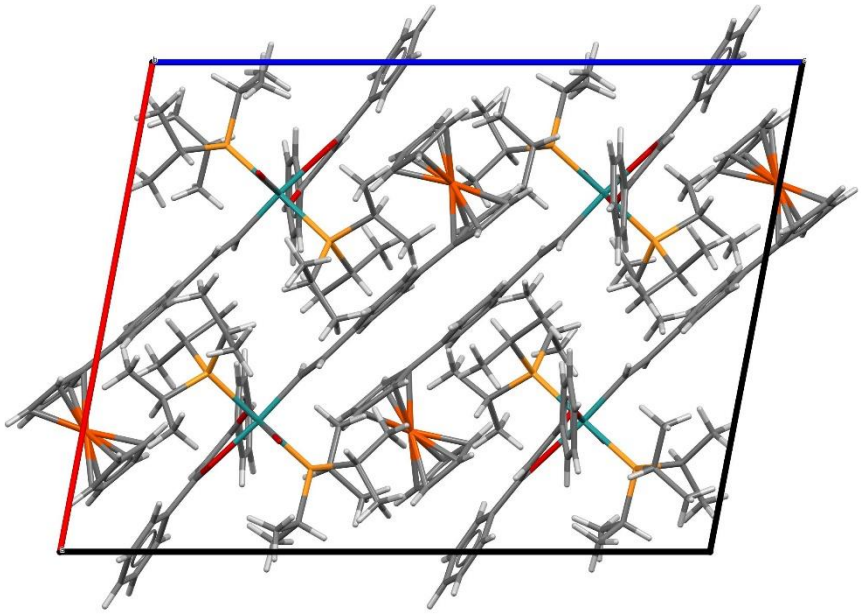

Figure S18. Packing of individual molecules in the crystal of complex **2-H**.

## Electrochemistry

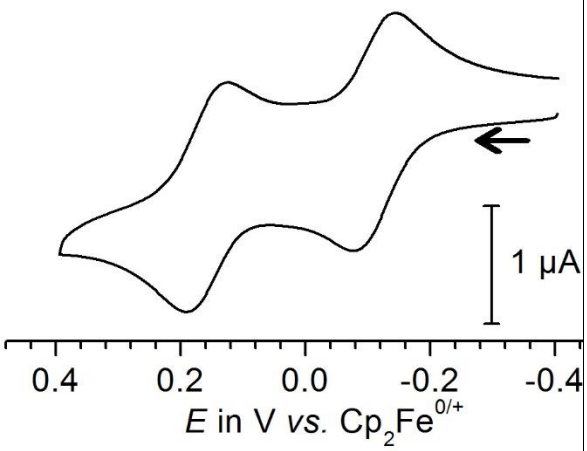


Figure S19. Cyclic voltammogram of **2-OMe** in $CH_2Cl_2$ / $NBu_4PF_6$ (0.1 M) at room temperature, scan rate *v* = 100 mV/s.

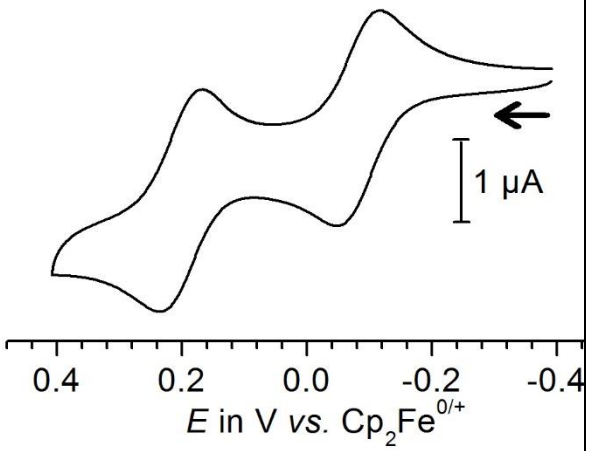


Figure S20. Cyclic voltammogram of **2-F** in $CH_2Cl_2$ / $NBu_4PF_6$ (0.1 M) at room temperature, scan rate *v* =100 mV/s.

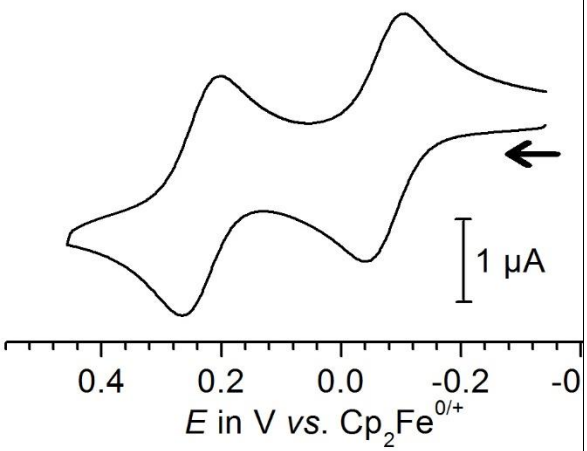


Figure S21. Cyclic voltammogram of **2-$CF_3$** in $CH_2Cl_2$ / $NBu_4PF_6$ (0.1 M) at room temperature, scan rate *v* = 100 mV/s.

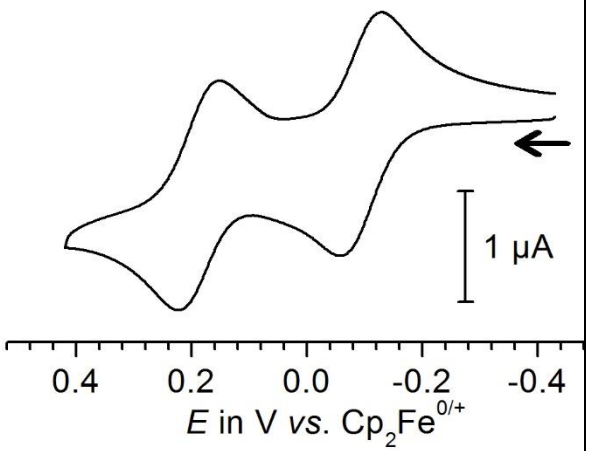


Figure S22. Cyclic voltammogram of **2-D** in $CH_2Cl_2$ / $NBu_4PF_6$ (0.1 M) at room temperature, scan rate *v* = 100 mV/s.

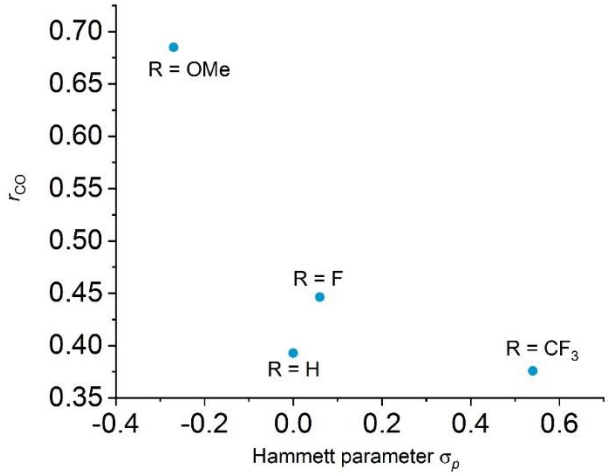


Figure S23. Plot of the σ-Hammett parameter of the substituents at the phenyl rings of the ketoenolato ligands *versus* $r_{CO}$.

## Quantum chemistry

Table S1. Percentage of the MO coefficient contributions of the three complex entities to the HOMO of the neutral complexes calculated by population analysis (6-31G(d)/pbe1pbe level of theory).

| | **Ru(CO)Cl($P^iPR_3$)$_2$(acac)** | **styryl** | **Fc** |
|---|---|---|---|
| **2-OMe** | 37 | 54 | 9 |
| **2-H** | 36 | 54 | 10 |
| **2-$CF_3$** | 32 | 55 | 13 |

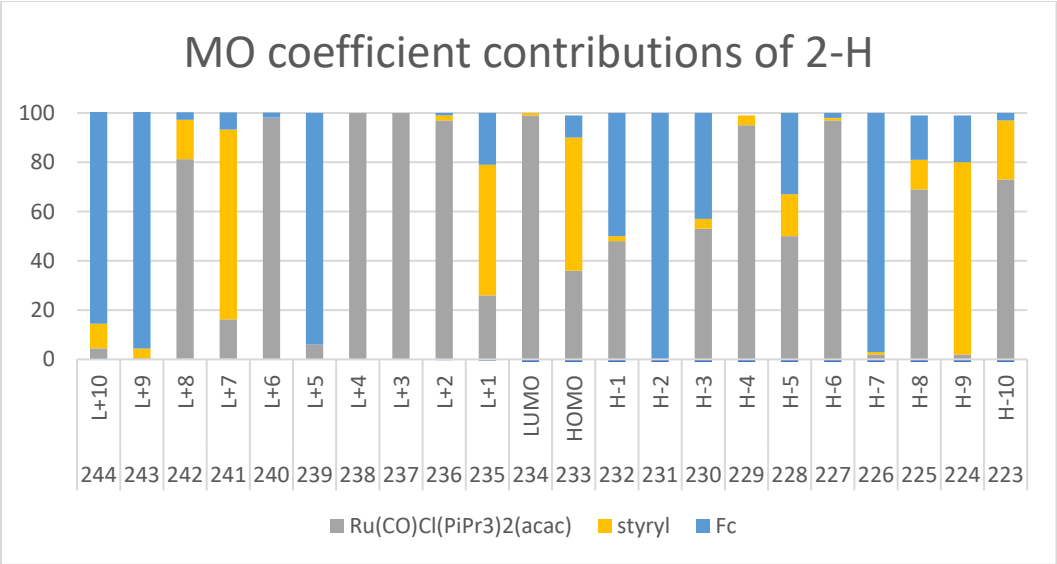


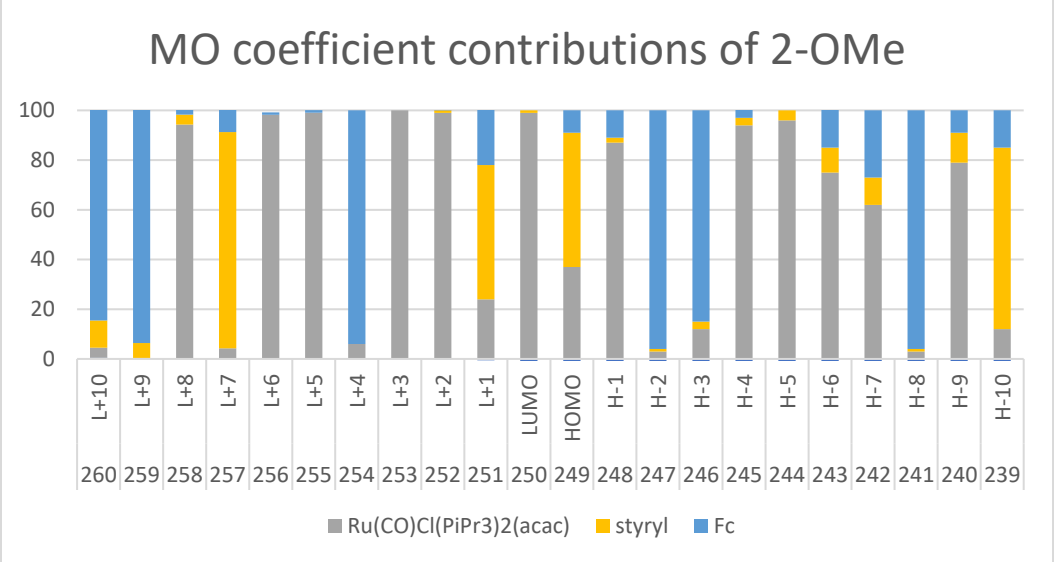


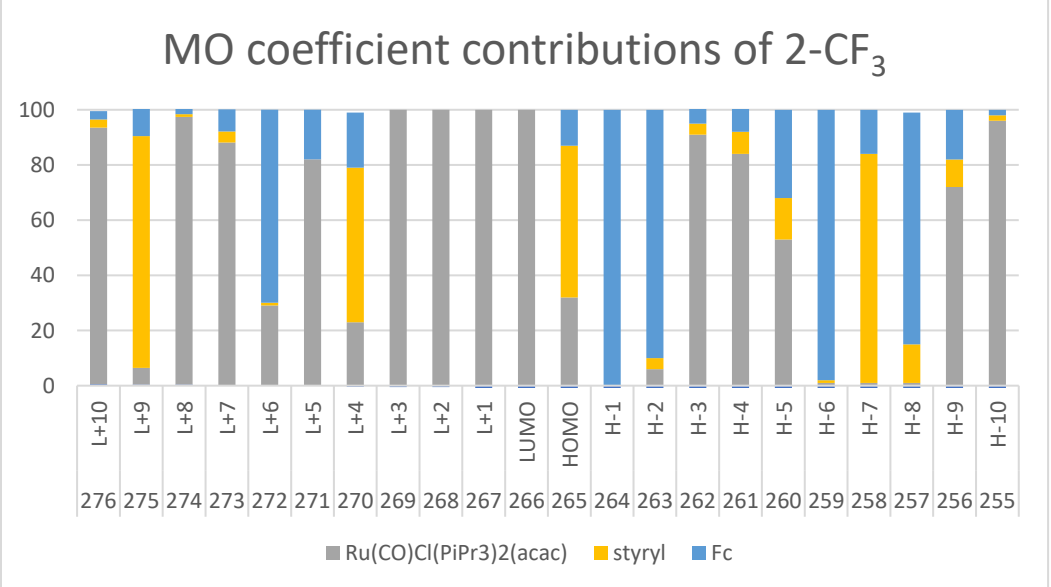


Figure S24. Compositions of MOs HOMO-10 to LUMO+10 for complexes **2-H**, **2-OMe** and **2-CF$_3$**.

## Temperature- and solvent-dependence of the IR and NIR spectra

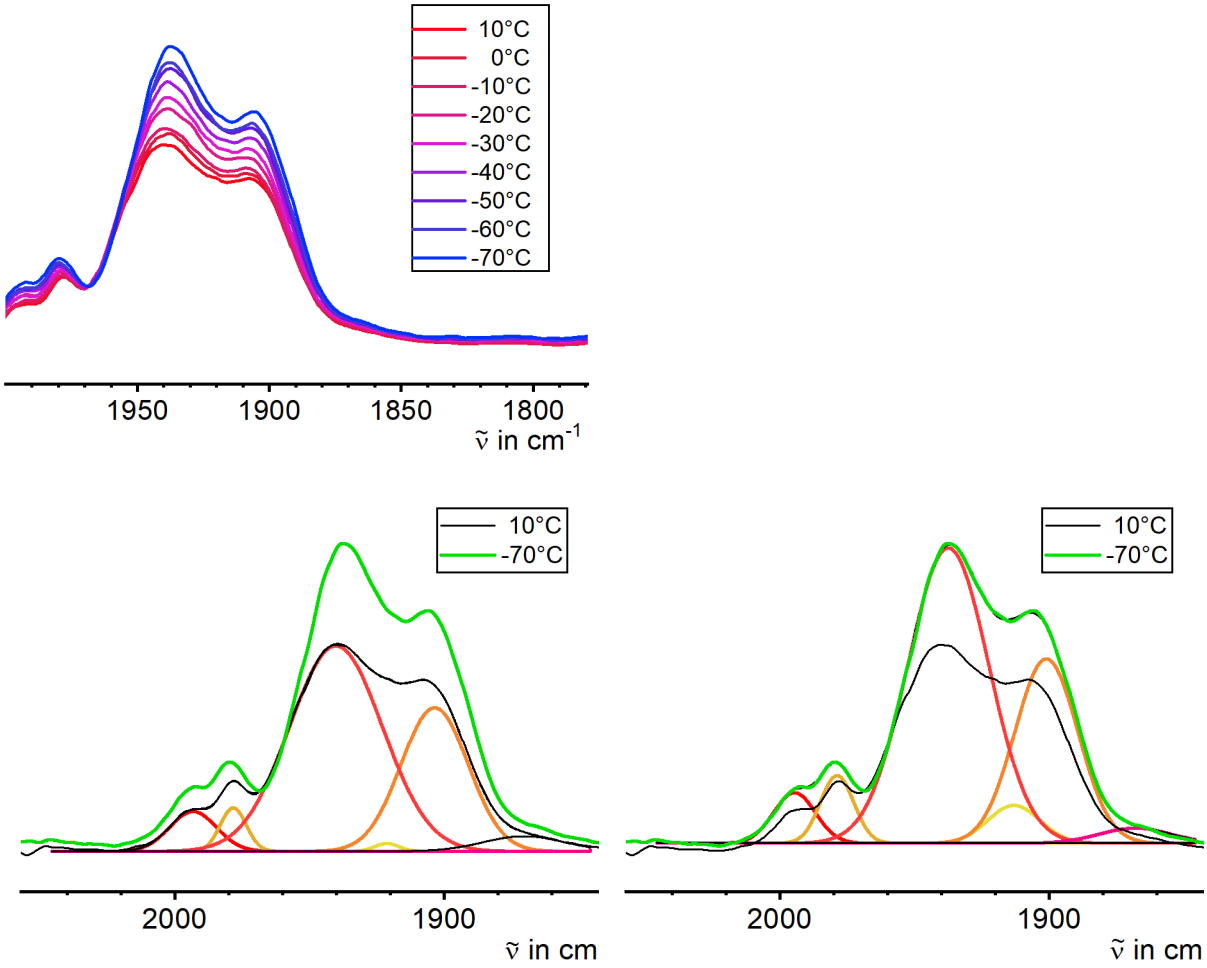


Figure S25. *T*-dependent IR spectra of **2-OMe•+** in the range of the Ru(CO) stretching vibrations over a temperature range of +10 °C to -70 °C (top). Deconvolution of the spectrum at *T* = 10 °C (left) and *T* = -70 °C (right).

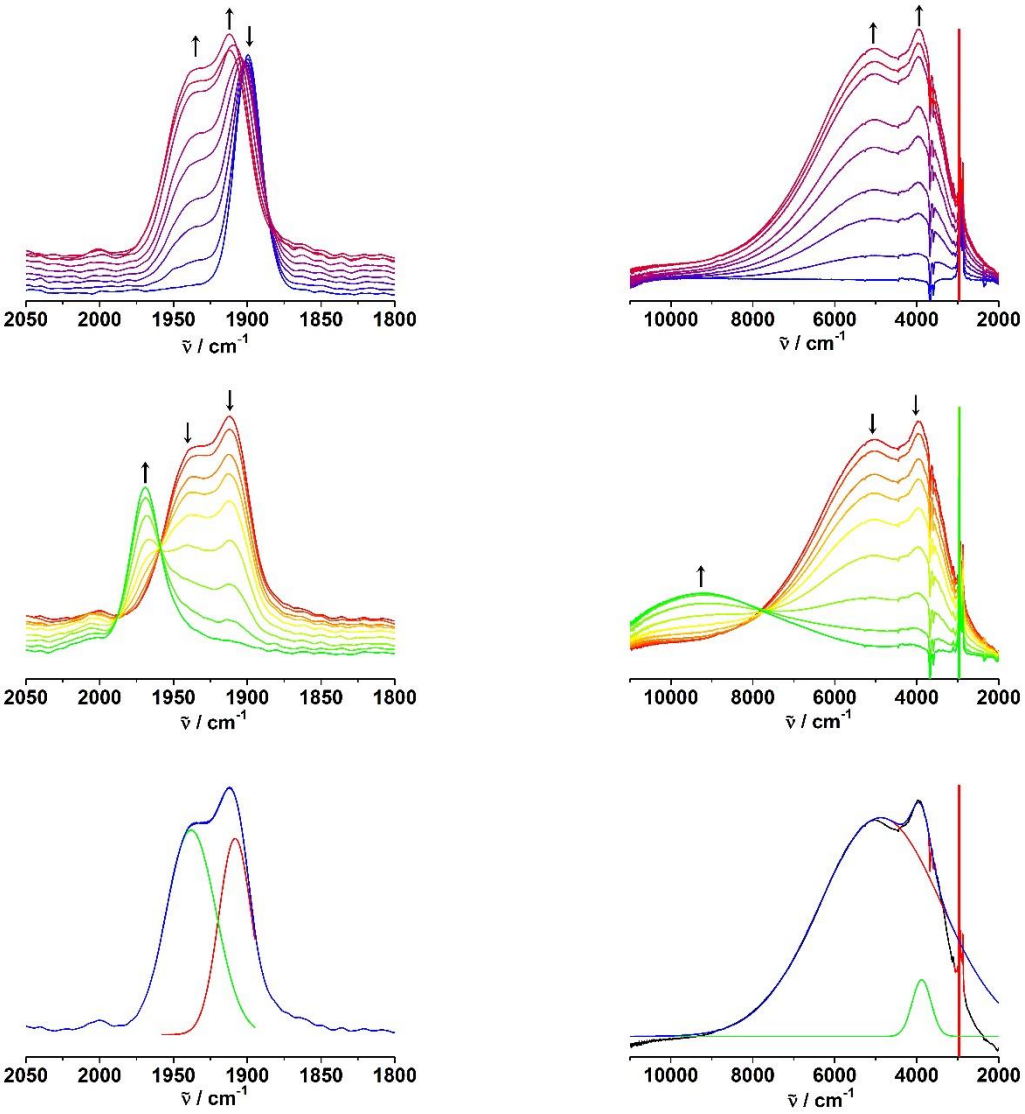


Figure S26. IR and NIR spectroelectrochemistry of **2-H** in 1,2-dichloroethane/$NBu_4PF_6$ (0.1 M) at room temperature and the deconvolution of the two-band pattern in the IR and NIR regions. Top and middle panel: blue = neutral, red = radical cation, green = dication. Bottom: Red and green lines represent the two Gaussians and the blue line their sum; the black line represents the experimental spectrum.

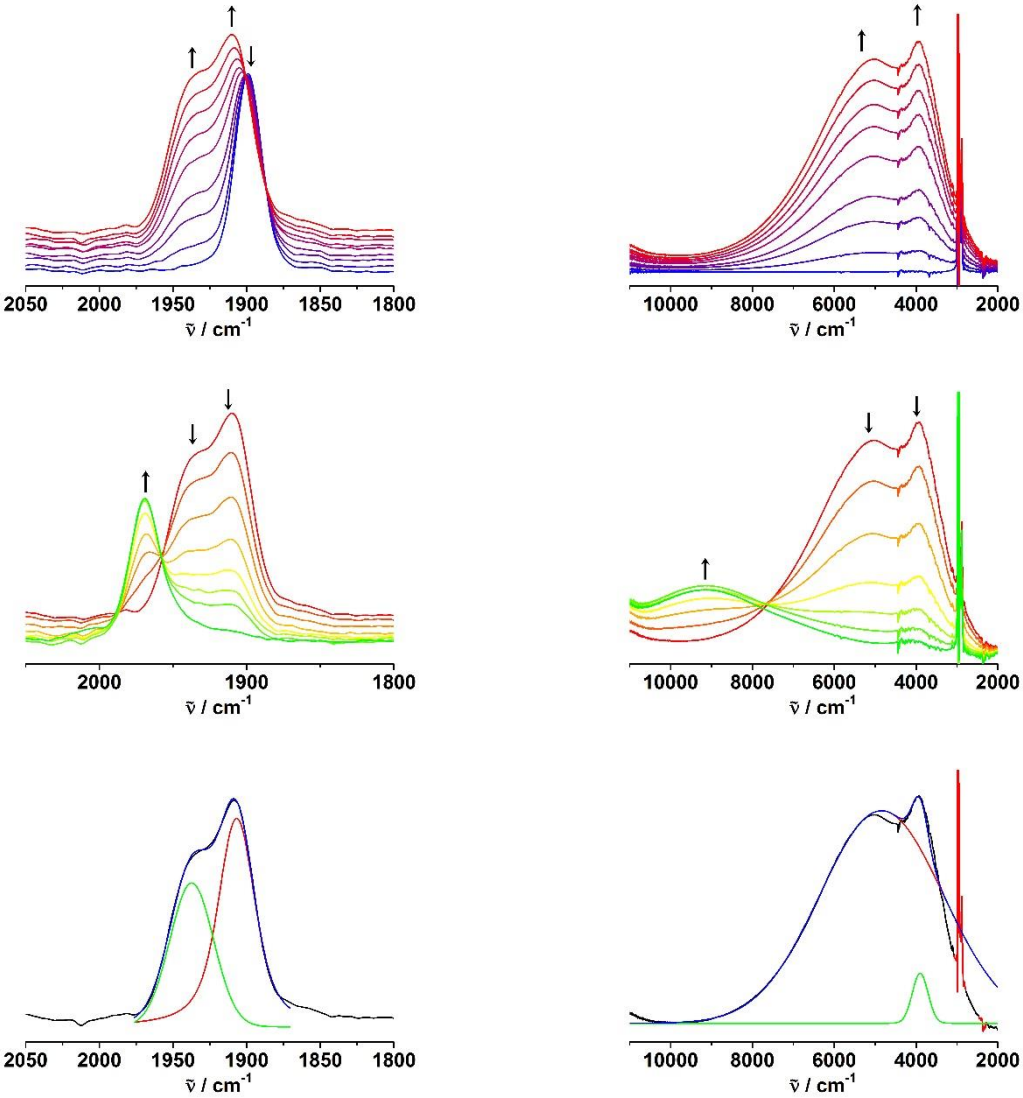


Figure S27. IR and NIR spectroelectrochemistry of **2-D** in 1,2-dichloroethane/$NBu_4PF_6$ (0.1 M) at room temperature and the deconvolution of the two-band pattern in the IR and NIR region. Top and middle panel: blue = neutral, red = radical cation, green = dication. Bottom: Red and green lines represent the two Gaussians and the blue line their sum; the black line represents the experimental spectrum.

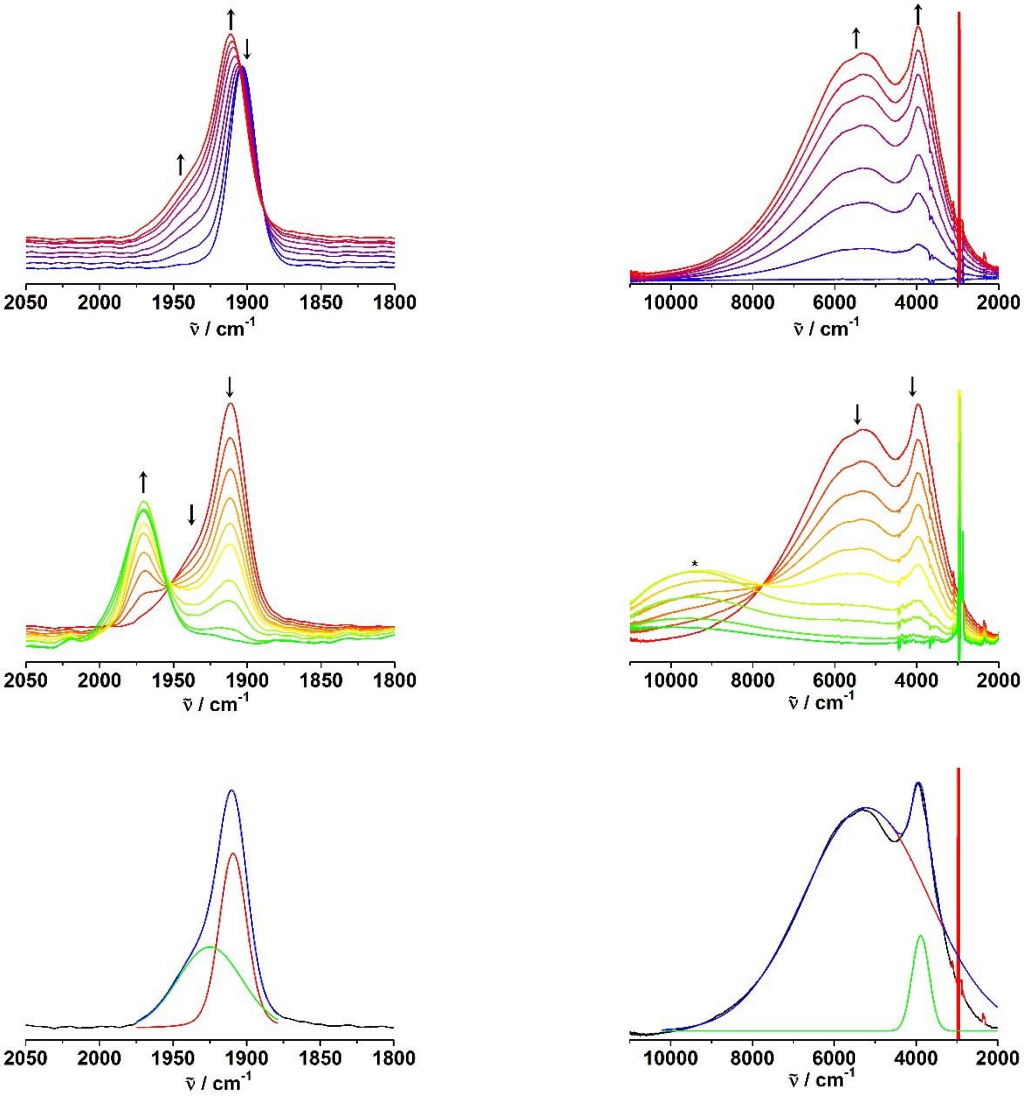


Figure S28. IR and NIR spectroelectrochemistry of **2-$CF_3$** in 1,2-dichloroethane/$NBu_4PF_6$ (0.1 M) at room temperature and the deconvolution of the two-band pattern in the IR and NIR region. Top and middle panel: blue = neutral, red = radical cation, green = dication. Bottom: Red and green lines represent the two Gaussians and the blue line their sum; the black line represents the experimental spectrum.

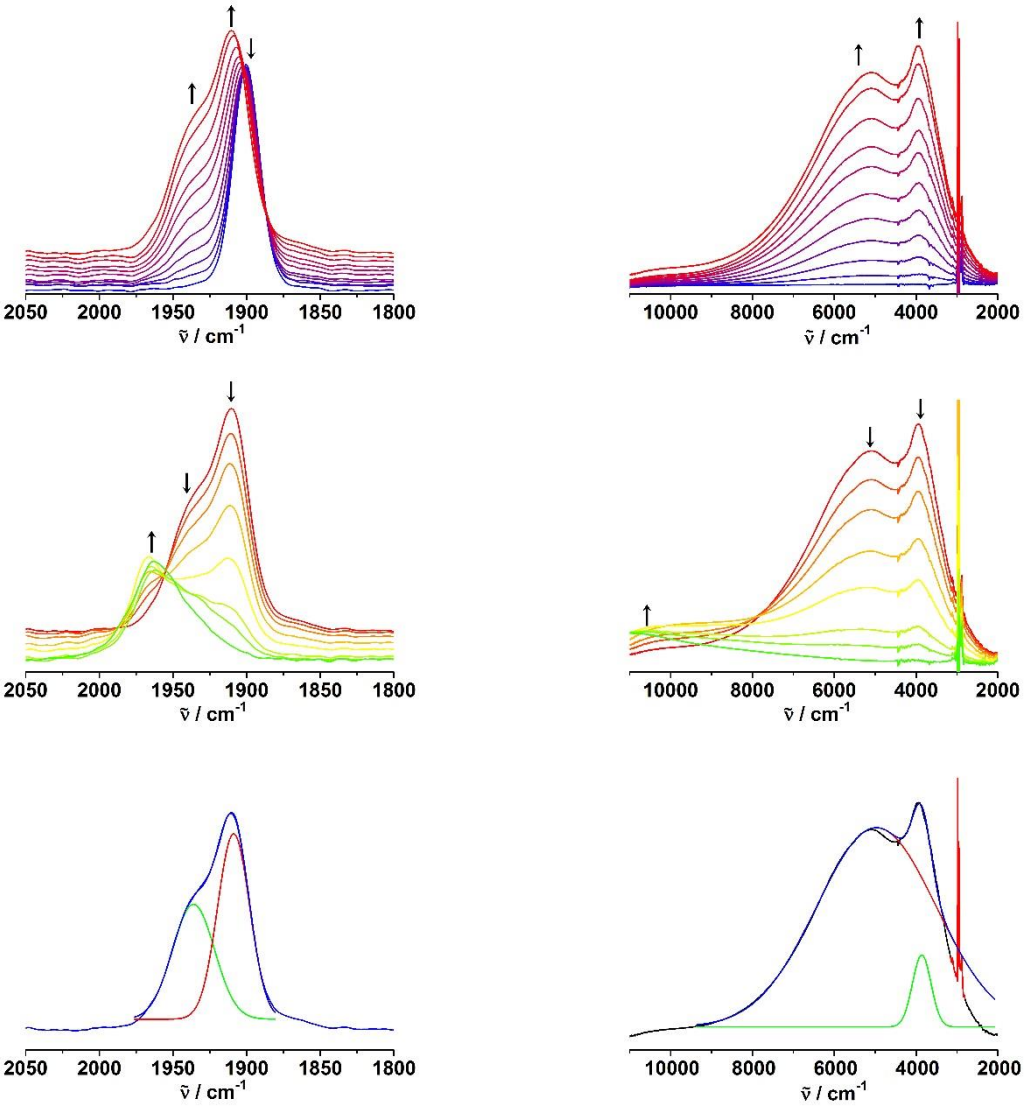


Figure S29. IR and NIR spectroelectrochemistry of **2-F** in 1,2-dichloroethane/$NBu_4PF_6$ (0.1 M) at room temperature and the deconvolution of the two-band pattern in the IR and NIR region. Top and middle panel: blue = neutral, red = radical cation, green = dication. Bottom: Red and green lines represent the two Gaussians and the blue line their sum; the black line represents the experimental spectrum.

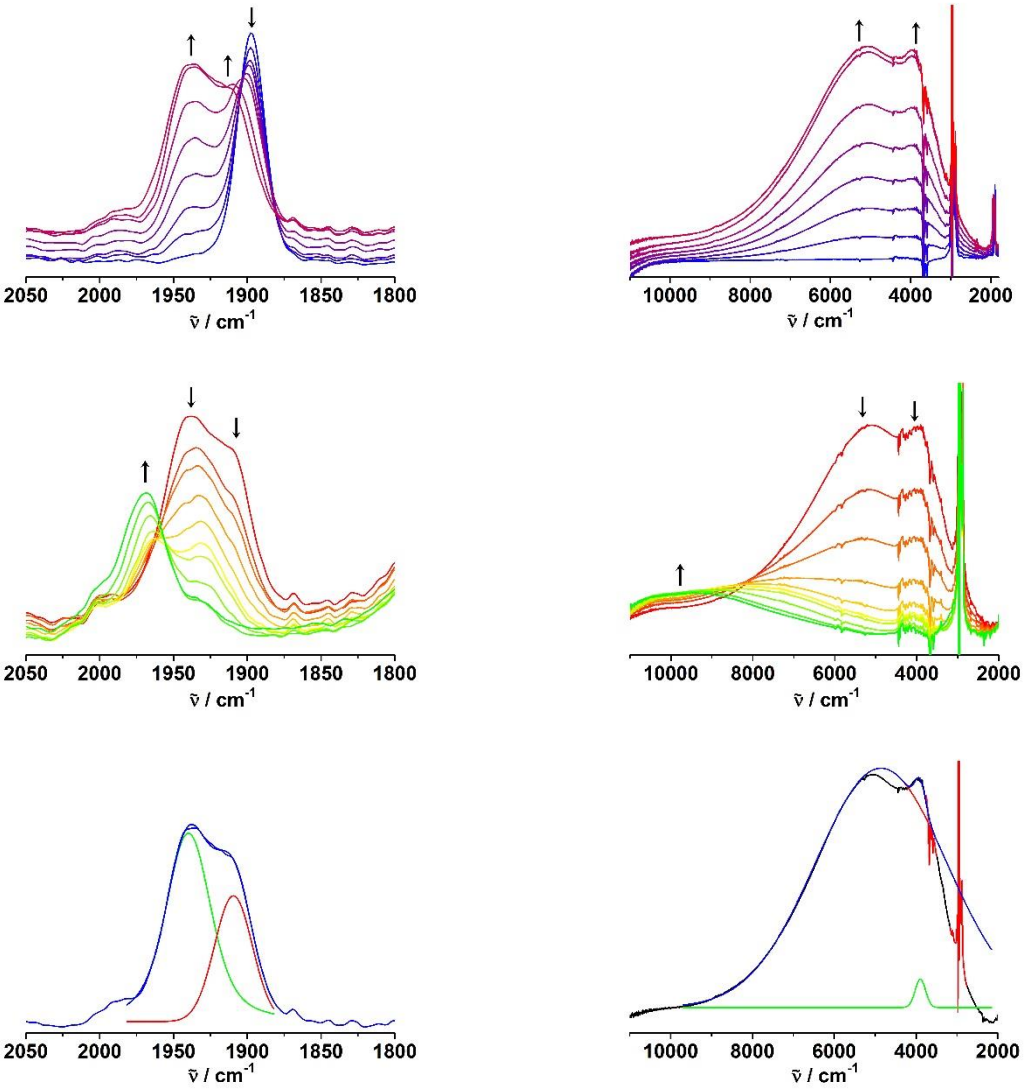


Figure S30. IR and NIR spectroelectrochemistry of **2-OMe** in 1,2-dichloroethane/$NBu_4PF_6$ (0.1 M) at room temperature and the deconvolution of the two-band pattern in the IR and NIR region. Top and middle panel: blue = neutral, red = radical cation, green = dication. Bottom: Red and green lines represent the two Gaussians and the blue line their sum; the black line represents the experimental spectrum.

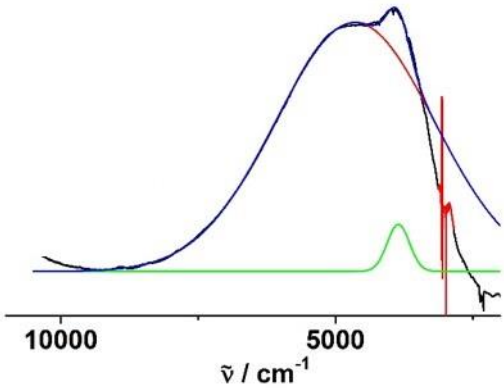


Figure S31. NIR spectrum of the [B{$C_6H_3(CF_3)_2$-3,5}]$^-$ salt of cation **2-OMe$^+$** in dichloromethane.

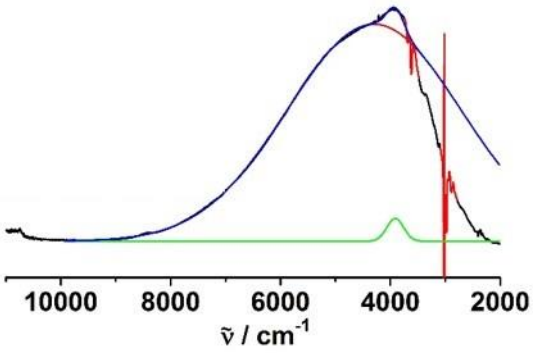


Figure S32. NIR spectrum of the [B{$C_6H_3(CF_3)_2$-3,5}]$^-$ salt of cation **2-OMe$^+$** in chloroform with deconvolution.

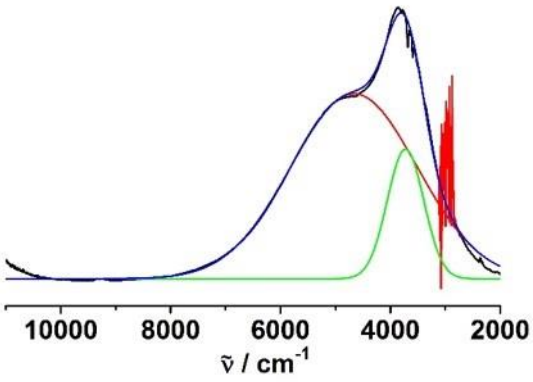


Figure S33. NIR spectrum of the [B{$C_6H_3(CF_3)_2$-3,5}]$^-$ salt of cation **2-OMe$^+$** in toluene with deconvolution.

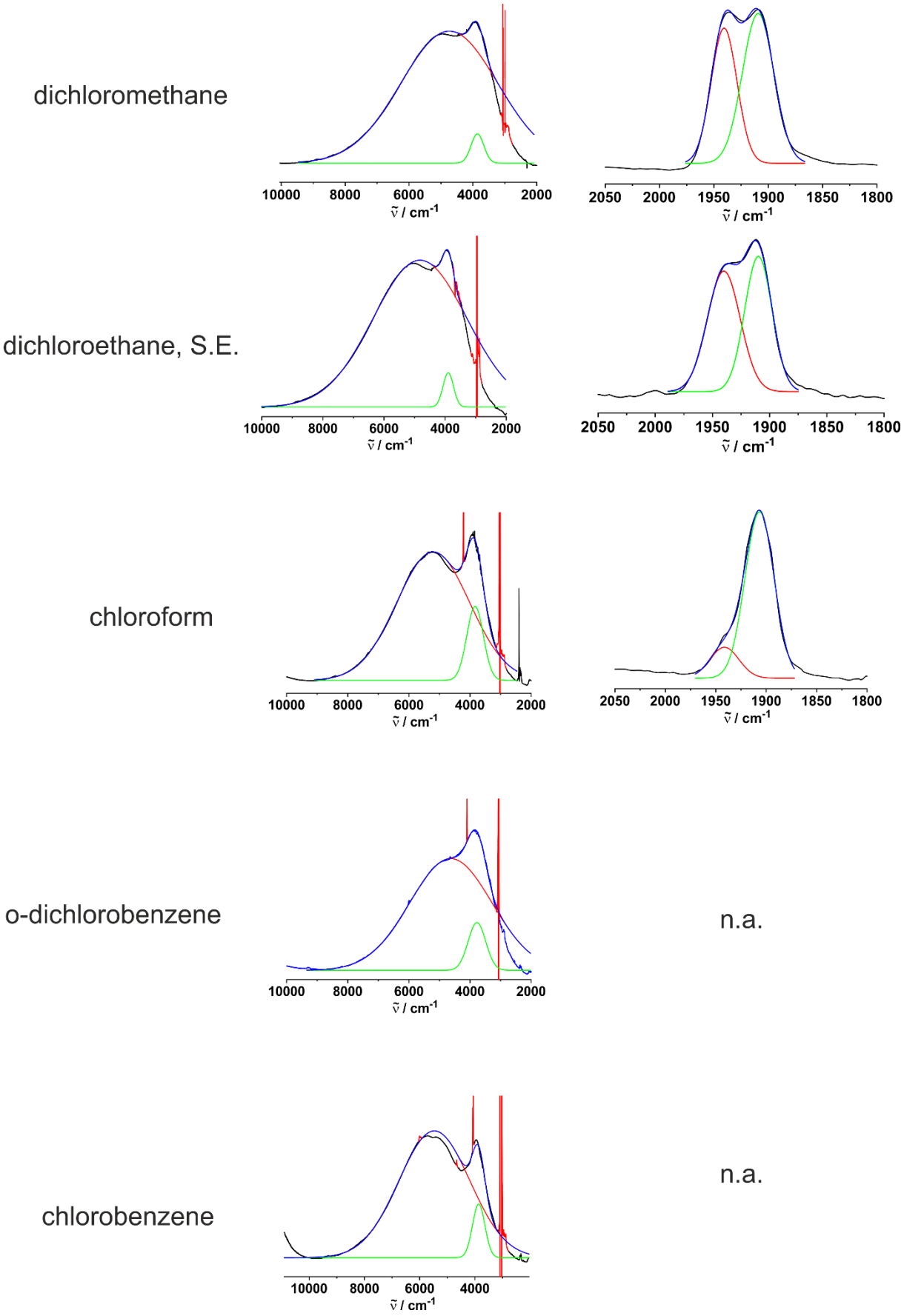


Figure S34. Study of the solvatochromism of **2-H$^+$**. NIR and IR spectra in the region of the CO-stretching vibrations with deconvolutions.

Table S2. Data from deconvolution of the NIR spectrum of the $PF_6^-$ salt of **2-OMe$^+$** in different solvents

| **Solvent** | **FWHM high energy** | **FWHM low energy** | **dielectric constant** |
|---|---|---|---|
| chloroform | 2809 | 638 | 4.81 |
| chlorobenzene | 3033 | 531 | 5.62 |
| dichloromethane | 3567 | 469 | 8.93 |
| o-dichlorobenzene | 3164 | 678 | 9.93 |
| dichloroethane, S.El. | 3601 | 405 | 10.36 |

Table S3. Data from deconvolution of the NIR spectrum of the $[B\{C_6H_3(CF_3)_2\text{-}3,5\}]^-$ salt of **2-OMe$^+$** in different solvents (FWHM = full-width at half-height)

| **Solvent** | **FWHM high energy** | **FWHM low energy** | **dielectric constant** |
|---|---|---|---|
| toluene | 2703 | 781 | 2.38 |
| $OEt_2$ | 3168 | 590 | 4.33 |
| chloroform | 3717 | 363 | 4.81 |
| chlorobenzene | 3353 | 606 | 5.62 |
| dichloromethane | 3383 | 477 | 8.93 |
| o-dichlorobenzene | 3456 | 543 | 9.93 |

Table S4. $r_{CO}$ and NIR solvatochromism of **2-H$^+$** ($r_{CO}$ = ratio of the peak area of the CO band at the higher energy to the total CO band intensities as defined by eq. 1.)

| **solvent** | $r_{CO}$ | **Energy of the NIR bands [cm$^{-1}$]** |
|---|---|---|
| dichloromethane | 0.40 | 4738+3857 |
| chloroform | 0.16 | 5205+3835 |
| dichloroethane, S.E. | 0.52 | 4823+3899 |
| chlorobenzene | n.a. | 5467+3861 |
| o-dichlorobenzene | n.a. | 4629+3774 |

## UV/Vis/NIR spectroelectrochemistry

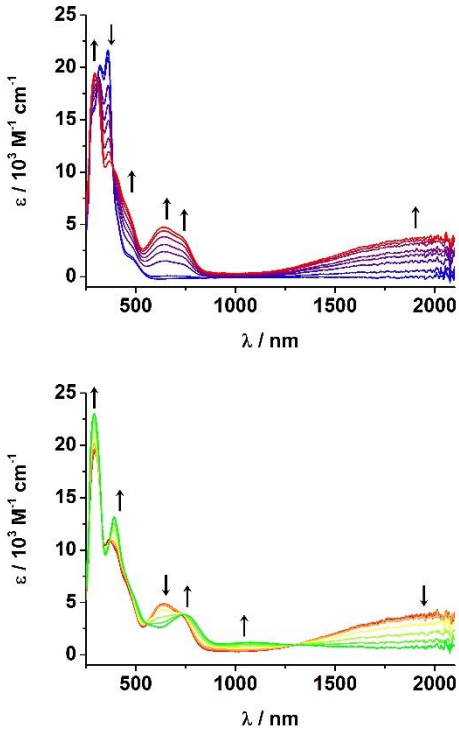


Figure S35. UV/vis/NIR spectroelectrochemistry of complex **2-H** in 1,2-dichloroethane/ $NBu_4PF_6$ (0.1 M) at room temperature (blue line = neutral complex, red line = radical cation, green line = dication).

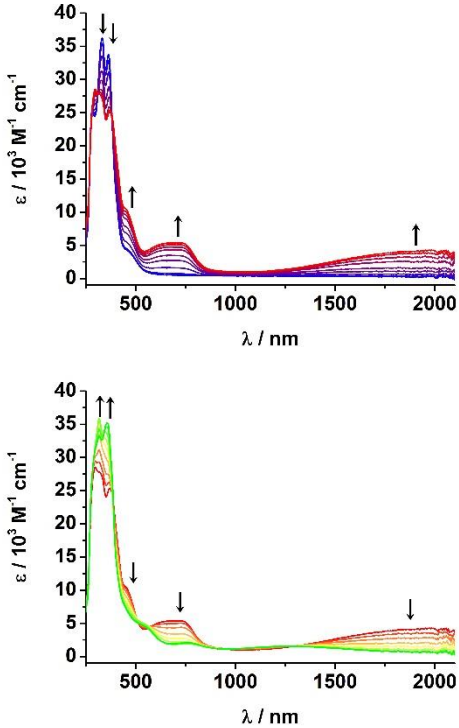


Figure S36. UV/vis/NIR spectroelectrochemistry of complex **2-OMe** in 1,2-dichloroethane/ $NBu_4PF_6$ (0.1 M) at room temperature (blue line = neutral complex, red line = radical cation, green line = dication).

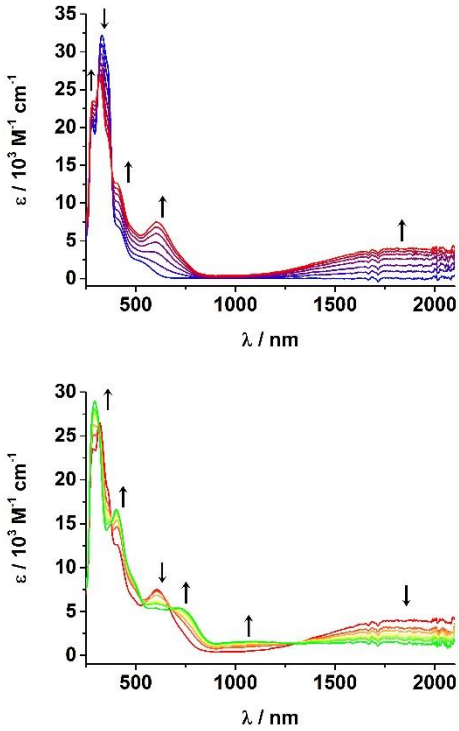


Figure S37. UV/vis/NIR spectroelectrochemistry of complex **2-$CF_3$** in 1,2-dichloroethane/ $NBu_4PF_6$ (0.1 M) at room temperature (blue line = neutral complex, red line = radical cation, green line = dication).

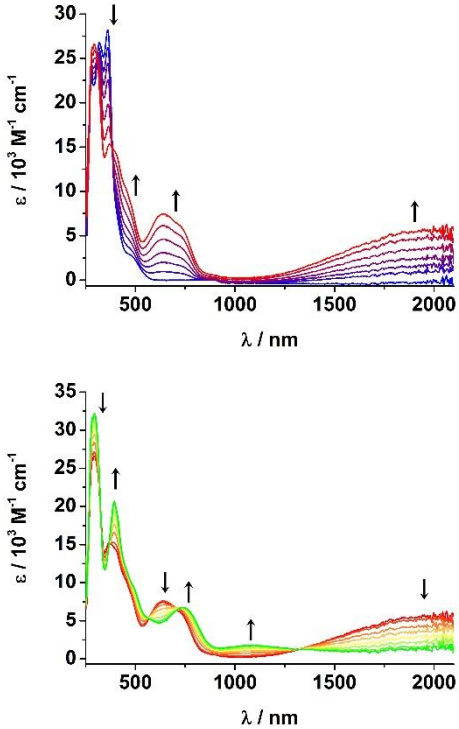


Figure S38. UV/vis/NIR spectroelectrochemistry of complex **2-D** in 1,2-dichloroethane/ $NBu_4PF_6$ (0.1 M) at room temperature (blue line = neutral complex, red line = radical cation, green line = dication).

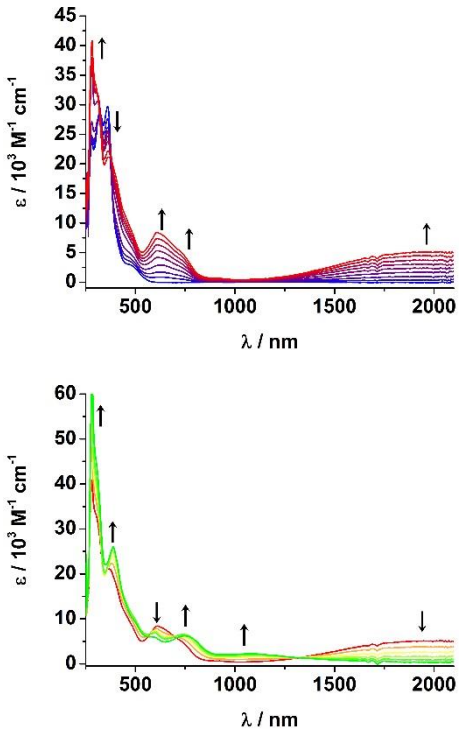


Figure S39. UV/vis/NIR spectroelectrochemistry of complex **2-F** in 1,2-dichloroethane/ $NBu_4PF_6$ (0.1 M) at room temperature (blue line = neutral complex, red line = radical cation, green line = dication).

## EPR spectra

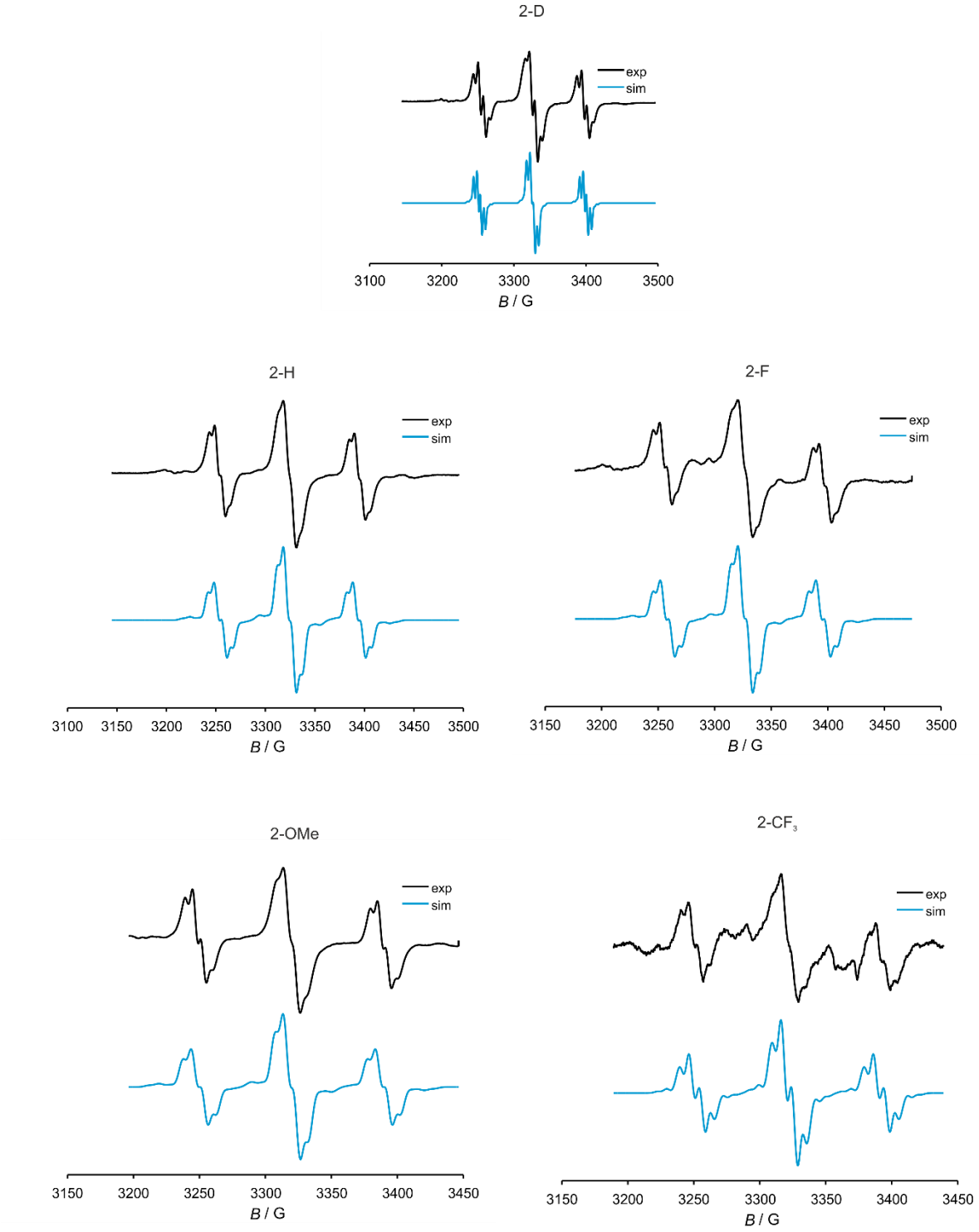


Figure S40. EPR spectra of the radical cations of the complexes at room temperature (black lines) and simulated spectra (blue lines).

## Mößbauer spectra

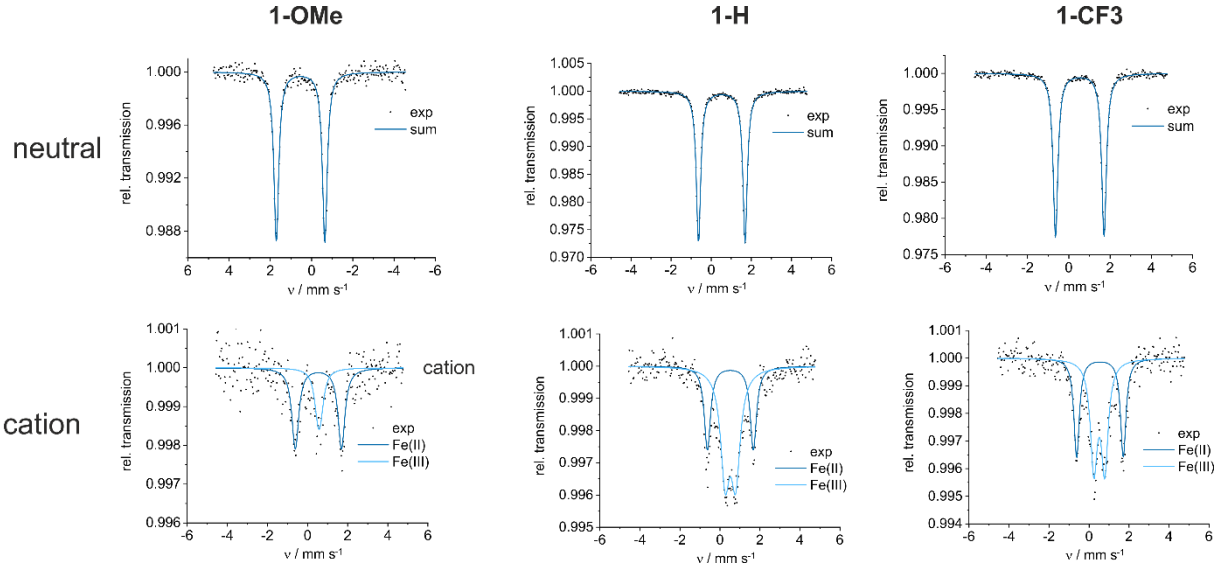


Figure S41. Mößbauer spectra of complexes **2-OMe**, **2-H**, and **2-CF$_3$** in their neutral (top) and radical cationic forms (bottom) at 80 K, referenced against $\alpha$-Fe.

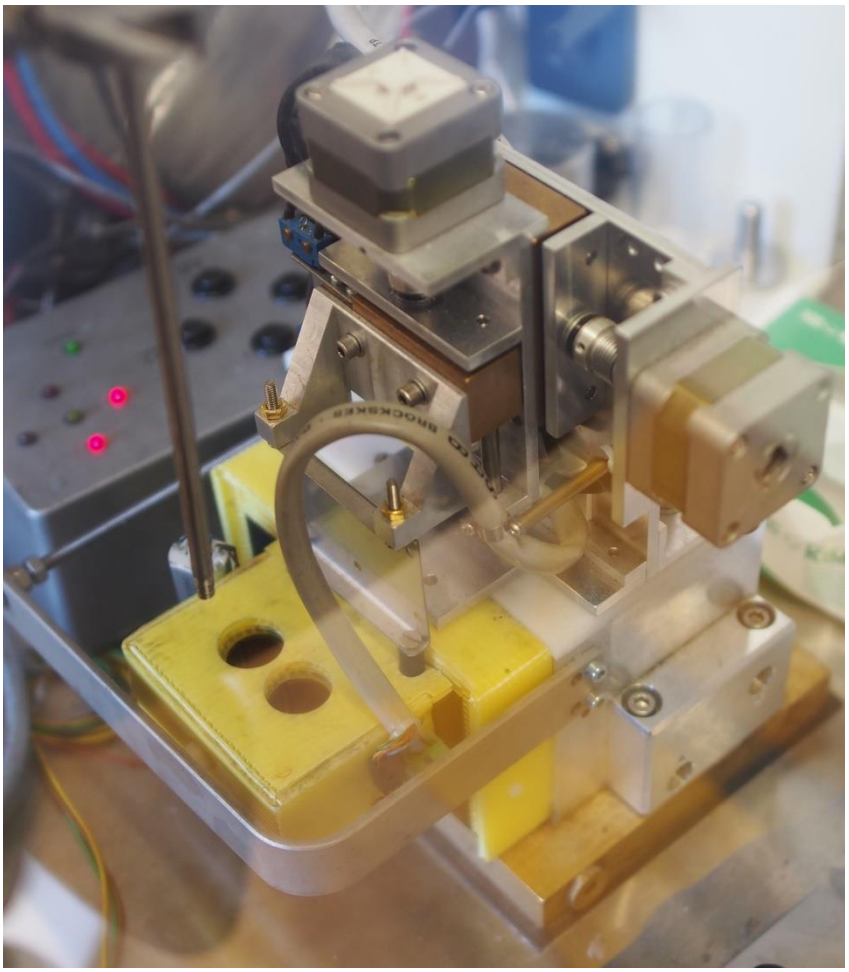

Figure S422. Photography of the setup used for the acquisition of *T*-dependent IR spectra.